Cross Sarah (Orcid ID: 0000-0003-4298-9307)
Pettigrew Ross P. (Orcid ID: 0000-0001-5664-6765)
Priddy Charlotte (Orcid ID: 0000-0002-3007-1374)
Zuchuat Valentin (Orcid ID: 0000-0002-2029-6422)
Dodd Thomas J.H. (Orcid ID: 0000-0003-2257-6740)
Mitten Andrew (Orcid ID: 0000-0002-0526-0368)

The sedimentological expression of transgression-regression cycles upon aeolian-marine margins

Cross, S.[1]; Pettigrew, R.P.[1]; Priddy, C.L.[1*]; Zuchuat, V.[2]; Dodd, T.J.H.[1&3]; Mitten, A.J.[1]; Clarke, S.M.[1]

[1]Basin Dynamics Research Group, School of Geography, Geology and the Environment, William Smith Building, Keele University, Keele, Staffordshire, UK, ST5 5BG.

[2]Geological Institute, Faculty of Georesources and Materials Engineering, RWTH Aachen University, Wüllnerstrasse 2, 52062 Aachen, Germany

[3]British Geological Survey, The Lyell Centre, Research Avenue South, Edinburgh, UK, EH144AP.

[*]Present address: Department of Geology & Geophysics, University of Aberdeen, Aberdeen, UK, AB24 3UE

Corresponding Author Details

Cross Sarah; Basin Dynamics Research Group, School of Geography, Geology, and the Environment, Keele University; 09.sarah.cross@gmail.com

Pettigrew, Ross; Basin Dynamics Research Group, School of Geography, Geology, and the Environment, Keele University; ross.pettigrew@gmail.com

Priddy, Charlotte; Department of Geology & Geophysics, University of Aberdeen; Basin Dynamics Research Group, School of Geography, Geology, and the Environment, Keele University; charlotte.priddy@abdn.ac.uk

Zuchuat, Valentin; RWTH Aachen University Faculty of Georesources and Materials Engineering, Geological Institute; University of Oslo Faculty of Mathematics and Natural Sciences, Geological Institute; valentin.zuchuat@emr.rwth-aachen.de

This article has been accepted for publication and undergone full peer review but has not been through the copyediting, typesetting, pagination and proofreading process which may lead to differences between this version and the Version of Record. Please cite this article as doi: 10.1002/dep2.225

Dodd, Thomas; British Geological Survey- Edinburgh Office, Energy Systems and Basin Analysis; Basin Dynamics Research Group, Keele University, School of Geography, Geology, and the Environment; tdodd@bgs.ac.uk

Mitten, Andrew; Basin Dynamics Research Group, School of Geography, Geology, and the Environment, Keele University; Andrew.mitten@rhul.ac.uk

Clarke, Stuart; Basin Dynamics Research Group, School of Geography, Geology, and the Environment, Keele University; s.m.clarke@keele.ac.uk

Abstract

When compared to their temperate coastal counterparts, sediments deposited and preserved along arid aeolian to shallow-marine margins remain relatively poorly understood, particularly at the scale of lithofacies units and architectural elements. These systems often record evidence for relative sea-level change within sedimentary basins. This work focusses on the Entrada-Curtis-Summerville formations that crop out in central eastern Utah, USA, and provides a detailed analysis of the aeolian Moab Member of the Curtis Formation (informally known as the Moab Tongue) that was impacted by cycles of marine transgressions and regression in the late Jurassic. This study utilises photogrammetry, sedimentary logging, and sequence-stratigraphical analysis techniques. Results indicate that four short-lived transgressive-regressive cycles are preserved within the Moab Member, followed by a broad regressive event recorded at the transition between the Curtis and Summerville formations. These cycles relate to changes in the relative sea level of the Sundance Sea and the deflation and expansion of the neighbouring aeolian dune field. During periods of normal regression, marine sediments displayed evidence of tidal and wave action, whereas the continental domain was characterised by the growth of the aeolian system. However, when regression occurred within optimal physiographic conditions such as a restricted, semi-

enclosed basin, and at sufficient magnitude to outpace erg expansion, this acted to shut-down bedform development and preservation. A rapid restriction of aeolian sediment availability and the inability of the dune field to recover resulted in the formation of deflationary sandsheets, arid coastal plain strata, and contemporaneous shallow-marine deposits that are starved of wind-sourced sediments. This study highlights how a rapidly-developing high-magnitude regression can lead to the overall retraction of the erg. Deciphering the evolution and sequence stratigraphical relationships of arid aeolian to shallow marine margins is important in both understanding environmental interactions and improving the characterisation of reservoir rocks deposited in these settings.

Keywords: coastal margin, Curtis-Summerville formations, sequence stratigraphy, Utah

1 Introduction

Many aeolian successions comprise vast and apparently homogeneous deposits, documenting millions of years of geological time, which is recorded within both the preserved successions and by the unconformities that separate them. Aeolian systems are subject to both allogenic and autogenic forcing,

when these systems interact with neighbouring fluvial, lacustrine and marine margins complex interbedded successions of aeolian, alluvial, lacustrine, coastal and shallow-marine deposits are produced (Langford 1989, Mountney & Jagger, 2004; Rodriguez-Lopez, 2008; Al-Masrahy & Mountney, 2015, Kemp et al., 2017, Zuchuat et al., 2019ab; Priddy & Clarke, 2020, 2021; Pettigrew et al., 2020, 2021).

Continental erg systems have been studied extensively (Bagnold, 1941; Wilson, 1972; Hunter, 1977; Porter, 1986; Peterson, 1988; Clemmensen & Blakey, 1989; Kocurek, 1991; Crabaugh & Kocurek, 1993; Carr-Crabaugh & Kocurek 1998; Jerram et al., 2000; Mountney & Thompson, 2002; Mountney, 2012; Kok et al., 2012; Rodríguez-López et al., 2014; Mesquita et al., 2021; Yu et al., 2021) and are known to deposit and preserve clastic sandstones, many of which possess favourable reservoir qualities. When identified within the subsurface these can be indicative of hydrocarbon and sedimentary geothermal reservoirs and can provide opportunities for the development of carbon capture, utilisation and storage (Taggart et al., 2010; Sass & Götz 2012; Yu et al., 2018; Scorgie et al., 2021; Chedburn et al., 2022). However, there are comparatively fewer studies focussing on the relationships between erg systems and surrounding coeval marginal environments (Rodriguez-Lopez et al., 2013, 2014). Early work focussed on the sedimentary facies observed within the contemporaneous aeolian-marine environments, along with their spatial relationships (Loope, 1981; Chan, 1989) and sedimentary architecture (Fryberger &, 1984; Huntoon & Chan, 1987). Later work considered autocyclic controls within aeolian-marine margins, such as the influence of a fluctuating water table on accumulation and architecture of coastal aeolian systems (Crabaugh & Kocurek, 1993; Kocurek et al., 2001), whereas, more recent studies have interpretated the aeolian-marine deposits in a sequence stratigraphic context and focussed on the complex influence of allocyclic controls, such as climate and sea-level change on the deposits (Rankey, 1997; Jordan & Mountney, 2010, 2012; Wakefield & Mountney, 2013; Campos-Soto et al., 2022). Therefore, a detailed study on the interactions between marine margin and continental depositional processes has the potential to improve predictive sedimentary models. This is especially important in the context of reservoir modelling as the spatial distribution of freshwater and basin geometries is controlled by a combination of the sedimentological complexity of arid coastal margins and associated highly variable topography (Kocurek et al., 2001; Rodríguez-

López et al., 2020) created by the influence of mudstones and other tidally-influenced or marginal fine-grained facies that often act as baffles and/or barriers to flow (Chandler, 1987, 1989; Svendsen et al., 2007; Henares et al., 2014).

The Entrada-Curtis-Summerville succession exposed in south-eastern Utah documents the evolution of an arid coastal erg system that interacts with a neighbouring shallow sea. The Curtis and Summerville formations were respectively deposited within, and next to, a narrow seaway that extended from the Sundance Sea during the Oxfordian Age (Kreisa & Moila, 1986; Caputo & Pryor, 1991; Wilcox & Currie, 2008; Zuchuat et al., 2018 and references therein), in which tidal resonance (Collins et al., 2018) temporarily developed during periods of optimal physiographical conditions (Zuchuat et al., 2022). During phases of amplified tidal forces, autogenic processes have the potential to overprint the stratigraphical signature of autocyclic processes (Zuchuat et al., 2019a). The sedimentary deposits of the Moab Member of the Curtis Formation represent clear examples of such complex palaeoenvironmental settings, and illustrate the potential implications associated with correlating tide-dominated shallow-marine and dry aeolian successions. Therefore, to investigate the complexities within such environments, this study will: (i) characterise and further understand the interactions of depositional processes at both local and regional scales; (ii) redefine the understanding of facies interactions upon aeolian to shallow-marine margins; (iii) decipher sea-level fluctuations across an aeolian to shallow-marine margin at the local and regional scales, and; (iv) compile the results into a sequence stratigraphical framework for aeolian-marine margins.

2 Geological Setting

This study details the sediments of Upper Jurassic Curtis and Summerville formations (*sensu* Gilluly & Reeside, 1928) of the San Rafael Group in southern Utah, USA (Figure 1B,D; Doelling, 2001; Doelling et al., 2015). The sediments of these formations were deposited in a marginal marine

setting, with a warm arid aeolian coastal system bordered by a shallow sea (Caputo & Pryor, 1991; Lucas et al., 1997; Lucas, 2014). The Moab Member of the Curtis Formation comprises deposits of a coastal erg which developed at the south-eastern edge of a NNE-SSW-oriented retro-arc foreland basin, known as the Utah-Idaho Trough (Bjerrum & Dorsey, 1995). During the Late Jurassic, the foreland basin was periodically flooded during the south-easterly expansion of the Sundance Sea (Imlay, 1952, 1980; Pipiringos & O'Sullivan, 1978; Kreisa & Moila, 1986; Caputo & Pryor, 1991; Anderson & Lucas, 1994; Brenner & Peterson, 1994; Wilcox & Curie, 2008; Thorman, 2011; Zuchuat et al., 2018, 2019a, 2019b, 2022; Danise et al., 2017, 2018, 2020).

Directly underlying the Entrada Formation, two shallow-marine lithostratigraphic rock units are recognised in the study area, the Carmel Formation and the Curtis Formation (Figure 1B). The older of these two units is the Middle Jurassic Carmel Formation (Gilluly & Reeside, 1928), which is predominantly composed of limestone and evaporites deposited as the Carmel Sea transgressed over the arid continental Temple Cap Formation during the Callovian Age (Doelling et al., 2013). The Dewey Bridge Member comprises well-stratified reddish to brownish aeolian and sabkha deposits equivalent to the marine Carmel Formation (Fossen, 2010). The stratigraphic relationships created by the marine Carmel Formation and the continental Temple Cap along a northern embayment of the Sundance Sea (Doelling et al., 2013) in the Middle Jurassic bears striking resemblance to the marine Curtis Formation and continental Moab Member/Summerville Formation that followed.

The overlying continental Entrada Sandstone Formation (Figure 1B,D; Gilluly & Reeside, 1928) was deposited under arid conditions following the regression of Carmel Sea until the subsequent flooding of the area by the Curtis Sea (Crabaugh & Kocurek, 1993; Peterson, 1994; Carr-Crabaugh & Kocurek, 1998; Hintze & Kowallis, 2009). The Entrada Sandstone comprises two sub-units: the wet aeolian dune deposits of the Slick Rock Member, and the peri-dune-field mottled sandstone and mud flat deposits of the informally known “earthy facies” (Witkind, 1988; Crabaugh &

Kocurek, 1993; Carr-Crabaugh & Kocurek, 1998; Mountney, 2012; Doelling et al., 2015) across which occasional and local terminal fluvial splays developed (Jennings, 2014; Hicks, 2011; Valenza, 2016; Gross et al., 2022). The Entrada Sandstone is capped by a regional polygenetic and heterochronous transgressive surface termed the J-3 'Unconformity' (Figure 1B; Pipiringos & O'Sullivan, 1978; for discussion see Zuchuat et al., 2019b), which defines the base of the Curtis Formation (Gilluly & Reeside, 1928).

The Curtis Formation comprises predominantly siliciclastic shoreface and tidal sediments deposited during a marine transgression-regression cycle in the early Oxfordian Age (Wilcox & Curie, 2008; Zuchuat et al., 2019a, 2019b) associated with the development of the Moab Member's coastal erg. The Curtis Formation is divided into three informal units: the lower, middle and upper Curtis. Sediments of the lower Curtis are coeval with those of the uppermost part of the neighbouring Entrada Sandstone and comprise laterally restricted upper shoreface to beach deposits, which grade-laterally into thinly-bedded heterolithic subtidal deposits (Zuchuat et al., 2018). The base of the middle Curtis corresponds to the prominent 'Major Transgressive Surface (MTS)' flooding surface, which can be traced from the north to the south of the San Rafael Swell, and east to the Utah-Colorado border where it merges with the J-3 'Unconformity' (Zuchuat et al., 2018). The middle Curtis consists of amalgamated subtidal channel sediments, sediments deposited by subtidal to intertidal dunes, and tidal flat deposits. These deposits are comparatively better sorted than the underlying lower Curtis (Zuchuat et al., 2018). The upper Curtis documents the return of heterolithic, thinly-bedded intertidal to supratidal deposits.

The aeolian deposits of the Moab Member have been interpreted previously as forming the uppermost member of the Entrada Sandstone (*i.e.*, Gilluly & Reeside 1928; Wright et al., 1962; Thompson & Stokes, 1970). However, the coastal dune deposits of the Moab Member have since been correlated to the shallow-marine middle and upper Curtis Formation (Figure 1B; Peterson, 1988; Caputo & Pryor, 1991; Doelling, 2002, 2013, 2015;

Zuchuat et al., 2018, 2019a, 2019b; Lockley 2021a, 2021b). Both the shallow-marine and continental parts of the Curtis Formation display regionally-extensive stratigraphic surfaces, dividing intervals consistent with 100 kyr and/or 405 kyr cycles of orbital forcing (Zuchuat et al., 2019a). The shallow-marine deposits of the Curtis Formation and the aeolian dunes of the Moab Member are overlain by the arid coastal plain deposits of the Summerville Formation (Gilluly & Reeside, 1928; Wright et al., 1962; Caputo & Pryor, 1991; Peterson, 1994; Doelling, 2001; Lucas, 2014).

3 Methodology

Five detailed sedimentary logs were collected between the town of Moab and the eastern limb of the San Rafael Swell monocline (Figures 1A,C and 2), forming a roughly 60 km long west-to-east transect, with a cumulative stratigraphic thickness of *ca* 108 m. Logs were correlated using the combined J-3 unconformity-MTS surface, which is marked by an erosive contact separating a thin purple palaeosol horizon of the topmost Entrada earthy facies from the overlying Moab Member aeolian dunes (Peterson & Pipiringos, 1979; Lucas & Anderson, 1998; Wilcox & Currie, 2008; Anderson, 2015; Maidment & Muxworthy, 2019). Correlation of other key surfaces such as bounding surfaces and potential supersurfaces (*sensu* Kocurek, 1988) following the unconformity facilitated the identification of major high-resolution sequence stratigraphic bounding surfaces, constraining the Moab Member and Curtis Formation successions within a sequence stratigraphic framework.

Sedimentary logs were combined with high-resolution unmanned aerial vehicle (UAV) photogrammetry to provide a 3D visualisation of the preserved aeolian successions. Aerial photographs were collected using a 'DJI Phantom 4 Pro' drone, which was flown along a horizontal axis, whilst allowing for 80% overlap between images at a near-parallel viewing angle (Bemis et al., 2014; Priddy et al., 2019; Howell et al., 2021). The UAV-based photogrammetry was completed at four separate localities (Figure 1A), and ground-based photogrammetry was used at Bartlett Wash

due to proximity to Moab Airport and aerospace restrictions, with care taken to reduce inaccuracies in scaling and parallax error. The models were processed using 'Agisoft Metashape™' and interpreted using 'Virtual Reality Geological Studio' (VRGS) 2020 version 2.52.1 (Hodgetts et al., 2007). Bounding surfaces were traced and set and foreset thicknesses were measured within the aeolian successions using VRGS.

4 Sedimentology

From the five sedimentary logs (Figure 2), fifteen facies were identified (Table 1), which relate to both subaerial and subaqueous processes. The facies have been grouped into six facies associations; sinuous-crested aeolian dune association, straight-crested aeolian dune association, aeolian sand sheet association, supratidal flat association, intertidal flat association, and subtidal to intertidal flat association (Table 2). A combination of the six facies associations describe sediments in three depositional facies belts, including a coastal aeolian dune field, a coastal plain, and a tide-dominated shallow marine margin.

4.1 Facies Associations

4.1.1 FA1 Sinuous Crested Dunes Facies Association

This Facies Association comprises tabular bodies with laterally extensive planar basal and upper bounding surfaces. Trough cross-bedded sandstones (*Stx*), arranged into 1-5 m thick sets with convex-up set bounding surfaces, comprises 95% of the association. Sweeping, asymptotic foresets comprise couplets of 3-10 cm thick, reverse-graded, fine to medium-grained sandstone with millimetre-scale very-fine grained laminae,

with a dominant transport direction towards the east. Toesets comprise pinstripe-laminated sandstones (*Spsl*) with the tops of the foresets truncated by the set bounding surfaces. The sets are arranged into 5-8 m thick cosets depicting similar transport directions and style of climb.

Sets of *Stx* with couplets of fine to medium-grained inverse graded sandstone and very fine-grained laminae represent the deposits of sinuous-crested wind-blown bedforms migrating by the processes of grainflow and grainfall (Crabaugh & Kocurek, 1993; Mountney, 2012; Banham et al., 2018). The presence of pinstripe-laminated sandstones along the dune toesets suggests strong winds, or at the very least winds with sufficient energy for traction to dominate in the lee of dune bedforms (Kocurek, 1991).

4.1.2 FA2 Straight Crested Dunes Facies Association

This Facies Association is characterised by tabular bodies up to 5 m thick, with laterally extensive planar basal and upper bounding surfaces. The majority of the association comprises planar cross-bedded sandstones (*Spx*) arranged into 0.5-1 m thick sets with low-angle planar set bounding surfaces. Sweeping, asymptotic foresets comprise couplets of inversely graded medium-grained sandstone with millimetre-scale very-fine-grained laminae, interbedded with finer-grained pinstripe laminated sandstones (*Spsl*). *Spsl* is also observed climbing up the toesets with the tops of the foresets truncated by the set bounding surfaces. Rhizoliths are sporadically preserved along the foresets, which when present are typically located towards the top of planar cross-bedded sets. The sets are arranged into 3-5 m thick cosets depicting a similar easterly transport direction and style of climb.

This association, comprising stacked planar cross-bedded sandstones (*Spx*) with low-angle planar laterally extensive bounding surfaces, is interpreted to be the deposits of straight crested aeolian dunes, which migrated by the combined processes of grainfall and grainflow (Trewin,

1993; Ewing & Kocurek, 2010; Collinson & Mountney, 2019). Pinstripe laminae along dune toesets suggests the winds had sufficient energy for traction to dominate in the lee of dune bedforms (Kocurek, 1991), and rhizolith development on foresets and towards set tops indicates primitive vegetation on the dune lee slope and dune crest.

4.1.3 FA3 Sand Sheet Facies Association

This Facies Association is characterised by laterally extensive sheet-like bodies with planar upper and lower bounding surfaces and a dominance of undulose bedded to structureless sandstones (*Su & Ss*) with extensive mottling and fluid escape structures. Trough cross-bedded sandstones (*Stx*) and pinstripe laminated sandstones (*Spsl*) are intermittently interbedded throughout the association with a typically mottled, poorly consolidated sandstone (*Pfg*) present at the top of the succession.

This association is interpreted as the deposits of a sand sheet formed by a lack of sediment availability, inhibiting bedform development. This is probably the result of fluctuations in the water table from being below to above the sediment surface, reducing the local availability of sediment being transported (Kocurek & Havholm, 1993; Kocurek & Lancaster, 1999; Mountney & Jagger, 2004). Undulose bedded sandstones with extensive fluid escape structures are interpreted as reflecting periods of high water table conditions that led to the illuviation and formation of a ferric gleysol (*Pfg*). The presence of trough cross-bedded sandstones indicate some localised sediment availability to develop singular aeolian bedforms at the sediment surface. However, the lack of bedform trains suggest an overall sediment starved regime.

4.1.3 FA4 Supratidal Flat Facies Association

This Facies Association comprises tabular bodies with planar bounding surfaces containing centimetre to decimetre-thick interbedded, parallel-laminated mudstones, siltstones, and sandstones (*Sltpl & Spl*) with sporadic mottling, poorly preserved burrows and cross-cutting gypsum veins, which accounts for 80-90% of the association. Lenticular beds of structureless sandstones with concave-up, often erosive basal surfaces (*Ss*), load casts and very sporadic rip-up clasts also present, along with isolated occurrences of decimetre to metre-scale trough cross-bedded sandstones (*Stx*) and a single occurrence of a red-brown planar-laminated gypsisol (*Pgpl*) at the top of the association, containing laminated, nodular and satin spar gypsum.

This association is interpreted to be the deposits of an arid supra-tidal flat. A fluctuating water table is further evidenced by red-brown siltstones in which gypsum precipitated, and a gypsisol developed, that are particularly prevalent in the upper most units of the association. Parallel-laminated siltstones and sandstones represent suspension settling of wind-blown particles, with the decimetre to metre-scale trough cross-stratified sandstones interpreted as the migration of isolated, sinuous-crested dune forms over this area of suspension settlement. Occasional structureless sandstones with an erosive base represent channelised flash deposition of high sediment loads (*c.f.* Zuchuat et al., 2019), which have, in some places, been turbulent enough to rip-up deposits of parallel-laminated siltstone.

4.1.4 FA5 Intertidal Flat facies association

This Facies Association is composed of planar-laminated siltstones (*Sltpl*) interbedded with undulous sandstones with ripple laminations and sporadic mud-draping (*Surl*), often overlain by well consolidated wavy-bedded sandstones with sporadic siltstone laminations (*Swb*), interbedded

with 20-50 cm thick discontinuous rippled siltstone (*Srpl*) facies. Towards the top of the facies association parallel-laminated siltstones (*Slti*) inversely grade into very fine grained sandstones, interbedded with planar-laminated sandstones (*Spl*).

This association is interpreted as the product of intertidal flat sedimentation produced by tidal fluctuations in water level (Kvale, 2012). The relatively sandstone-rich nature of the intertidal flat may be attributed to the sediment being derived from the dune field. Initial undulose sandstones represent wind-blown strata onto a rising water table forming wave-ripple bedforms that are sinuous and out-of-phase. As the tide continues to rise, inversely-graded siltstones (*Slti*) (with regards to laminae thickness) mark rising water levels whereby suspension is the dominant means of deposition (Zuchuat et al., 2018). Towards the top of the succession sandstone-prone facies dominate, leading to the development of sandstone intertidal flat type facies whereby planar-laminated sandstones are deposited under upper flow regime conditions.

4.1.5 FA6 Subtidal to Intertidal Flat facies association

This Facies Association is sandstone-dominated, and consists of tabular bodies of unidirectional ripple to herringbone cross-stratified sandstones (*Shcs*), often overlain by parallel-laminated, inversely-graded siltstones (*Slti*), grading into centimetre to decimetre-thick parallel-laminated sandstones (*Spl*). Towards the top of the association, alternating intervals of wavy-bedded (*Swb*) and flaser-bedded (*Sfb*) sandstones with single and double mud draping on ripple forms, and centimetre to decimetre-thick symmetrical ripple-cross-laminated sandstones (*Srpl*) are abundant.

The occurrence of ripples and parallel-stratification testify to an environment oscillating between lower and upper flow regimes, while the tabular nature of the strata indicates that the processes are homogeneous and active over a large area. The double and single mud drapes on the foresets of the wavy and flaser-bedded ripples and dunes of this facies association develop during periodic, short-lasting periods of low flow velocity

(Reineck & Wunderlich, 1968; Sato et al., 2011; Baas et al., 2016), which, coupled with the bidirectionality of the herringbone cross-stratified sandstone reflecting regular current reversals, suggest deposition in a subtidal to intertidal environment (Zuchuat et al., 2018; Philips et al., 2020), in which oscillatory currents occurred as a secondary process. The regular alternation of flaser and wavy beds is interpreted as the reflection of neap and spring tide-like cycles (Allen, 1984; Tessier, 2022). The resulting heterolithic wavy strata deposited during lower energy neap tide periods (as compared to higher energy flaser-bedding deposited during spring tides) is often more argillaceous and contains smaller bedforms.

4.2 Facies Belts

4.2.1 Coastal Aeolian Dune Field (CADF)

This facies belt comprises sinuous-crested aeolian dunes, straight-crested aeolian dunes and sandsheet associations. Three types of aeolian dune cosets have been identified: low-angle climbing straight-crested dune cosets, small low-angle climbing sinuous-crested dune cosets, and large low to moderate-angle climbing sinuous-crested dune cosets, which decrease in size and sinuosity towards the aeolian-marine margin. All of these cosets have large-scale flat to extremely low angle coset bounding surfaces that are discordant with underlying set, and foreset bounding surfaces and are typically lined with rootlets that penetrate up to 20 cm in a sub-parallel manner. In all coset types, the toesets of the dunes overlying the set-bounding surfaces show an abrupt contact and, in most cases, do not preserve the antecedent topography of the underlying dune sets.

The small low-angle climbing sinuous-crested dune cosets typically occur near the base of the facies belt, and contain dune sets that are *ca* 0.1-1 m thick, progressively increasing in thickness upwards, with set bounding surfaces often displaying changes in the angle of climb (Figure 3). The

larger, low to moderate-angle climbing, sinuous-crested dune cosets occur in the middle to upper portion of the coastal aeolian dune facies belt, and contain dune sets that are *ca* 0.5-3 m thick, again displaying a progressive increase in thickness upwards, with undulatory set-bounding surfaces (Figure 3). Finally, the low-angle climbing straight-crested dune cosets occur in two places within the facies belt: at the very base of the facies belt underneath the small sinuous-crested dunes, and towards the top of the facies belt, above the larger sinuous-crested dunes (Figure 3). They contain dune sets that are *ca* 1-2 m thick and have set-bounding surfaces that are planar to very low angle. The uppermost association within the facies belt comprises predominantly sandsheet associations with minor sinuous-crested aeolian dune associations. Blue-grey isolated gleysol facies, often with yellow staining permeating into the underlying units, are observed sporadically towards the top of the facies belt.

Interpretation

This facies belt is characterised as a coastal aeolian system, due to its spatial stratigraphic position (Peterson, 1988; Caputo & Pryor, 1991; Doelling, 2002, 2013, 2015; Lockley 2021a, 2021b) and proximity to coeval coastal plain and shallow marine environments. Sedimentological evidence supporting this interpretation is indicated by the presence of extensive aeolian dune development and the lack of preserved interdunal facies relative to the presence of substantial rooted and palaeosol horizons (Mountney, 2012). The abrupt contact between overlying dune toesets and underlying dune deposits indicates a lack of reworking at the sediment surface, and could be attributed to dry dune migration and climb. However, due to the described palaeosols and rooting this is more likely to be indicative of a damp substrate (Mountney & Thompson, 2002; Mesquita et al., 2021). Rhizolith development on coset-bounding surfaces suggests sub-aerial exposure for an amount of time sufficient for the development of vegetation and stabilisation of the dune field (Loope, 1988; Bullard, 1997).

The small sinuous-crested dunes, aggrading at a low angle of climb, are interpreted as immature dune development and the initiation of bedform trains (Mountney, 2006a, 2012). The gradually increasing angle of climb to the small sinuous-crested dunes, together with increasing set thickness up succession, indicates the increasing maturity of the dune train development. The presence of larger sinuous-crested dunes suggests more sediment was available to promote the development of greater aggradational angles and set thickness preservation (cf. Mountney, 2006a, 2006b, 2012; Cosgrove et al., 2022). The spatially discordant nature of the set surfaces indicates the joining, and cannibalisation of juxtaposing sinuous-crested dune forms, suggesting the potential development of compound dune morphologies. The development of straight-crested dunes indicates a lower sediment availability than that of the sinuous-crested dunes. However, with dune sizes and angles of climb being sufficient to preserve climbing metre-scale sets, dune train maturity must be inferred as a key process in their formation, in addition to relatively low sediment availability conditions (Kocurek & Havholm, 1993; Mountney, 2006a, 2006b, 2012). The sandsheet associations present at the top of the facies belt indicate a reduction in sediment availability for bedform development and deflation of aeolian dunes (Kocurek & Lancaster, 1999). The basal bounding surface of the sandsheet association potentially marks a deflationary surface due to the presence of rooting and some isolated palaeosols. The gleysols at the top of the sandsheet association may indicate a high water table for a sustained period of time allowing interstitial waters to illuviate the host sediment, producing a palaeosol (Lizzoli et al., 2021).

4.2.3 Coastal Plain (COPL)

This facies belt is dominantly composed of the supratidal flat association, with subordinate interbeds of intertidal flat and sandsheet associations, uniformly alternating between each with a relatively consistent thickness. The facies belt comprises poorly-consolidated but laterally extensive,

parallel-laminated mudstones and siltstones. Rare, isolated dunes and thick lenses of structureless sandstones, characterised by a concave upward erosive base often with load casts and a sharp flat top surface are also present. Gypsisol is common at the top of the facies belt, with frequent laminae, nodules, and veins of gypsum present in the west of the study area.

Interpretation

The facies belt is characterised as an arid coastal plain assemblage that reflects a transition away from an intertidal flat into a supratidal flat, with a decrease of tidal energy in a landward direction. This facies belt shows a widespread flat area, dominated by wind-blown sediments that lack bedform development. Thick deposits of erosive and structureless sandstones show evidence of storm event type influxes of sediment alternating with the thin laminated siltstones deposited as suspension settlement during periods of quiescence. Within this environment, deposits influenced by tidal forces occur sporadically, and represent only significant events that cause local sea-level to expand far enough inland, typically during extreme storm events (Kumar & Sanders, 1976; Storms, 2003). The gypsisols present near the top of the facies belt indicate a degree of water table draw-down via evapotranspiration within an arid saline environment (Jordán et al., 2004; Andeskie et al., 2018; Pettigrew et al., 2021).

4.2.5 Tide-Dominated Shallow-Marine Margin (TDMM)

The facies belt comprises the supratidal flat, intertidal flat and subtidal to intertidal flat associations, with the intertidal to supratidal flat associations commonly forming the top of the facies belt, conformably overlying the subtidal to intertidal association. The base of the facies belt comprises wave-ripple laminae, double and single mud drapes on ripple sets, and herringbone cross-stratification of the subtidal to intertidal flat zone (Figure 4). The overlying intertidal to supratidal zone depicts the dominance of typical tidal facies such as wavy and bi-directional flaser

bedding (Figure 4), along with a dominance of single mud drapes. Bioturbation is commonly observed, predominantly in the form of vertical burrows, which are absent in the other facies belts. The bedload sediments of this facies belt have a relatively uniform grainsize and are of a similar calibre to the sediments of the coastal dune field facies belt.

Interpretation

This facies belt is interpreted as a tide-dominated shallow-marine margin (TDMM) and is gradually and conformably overlain by the intertidal and supratidal deposits of the coastal plain facies belt. The generation of herringbone-cross stratification, single and double mud drapes, bi-directional flaser bedding, and wavy bedding indicates a flow regime of alternating energy (Rahman et al., 2009; McCrory & Walker, 1986; Bradley et al., 2018). Additionally, wave indicators preserved in the system suggest an efficient and consistent tidal reworking of such deposits (Olivero et al., 2008). The presence of flaser and wavy bedding occurs in relatively uniform grain sizes, indicating that the sediment source is relatively unimodal and well-sorted. This, coupled with the similarity between bedload dominated facies grain-size and the dry aeolian system, makes it a probable source of sedimentation. Burrowing trace fossils within this facies belt suggests a relatively calm environment with limited wave action (Yang et al., 2005). This is also indicated by the limited amount of scour observed within the facies belt, indicating a somewhat sheltered tide-dominated marine margin. It is possible that perennial fluvial system discharge variability in fully fluvial or estuarine settings could produce cyclical bedforms and sedimentary structures, not unlike the ones observed in this facies belt (Martinius & Gowland, 2011; Reesink & Bridge, 2011). However, the lack of such perennial fluvial systems preserved in the rock record, coupled with the abundance of tidal indicators such as bidirectional current ripples, double and single mud drapes, and tidal bundles (Kreisa & Moila, 1986), along with a physiography that can generate very amplified tidal currents (Zuchuat et al., 2022), indicates that tidal processes played an important role in the deposition of this facies belt.

5 Depositional model of the Curtis-Summerville aeolian-marine margin

5.1 Spatial interaction of the Curtis aeolian-marine margin

The Moab Member of the Curtis Formation is interpreted to be deposited within a dry-damp aeolian environment, which interacted with a tide-dominated shallow-marine margin setting (Figure 5A; Peterson, 1988; Caputo & Pryor, 1991; Doelling, 2002, 2015; Zuchuat et al., 2018, 2019a, 2019b). The coastal aeolian dune field comprising dunes and sand sheets is best-observed in the Bartlett Wash outcrop to the east of the study area (Figure 6), where the thickest measured section is also observed (Figure 2).

The percentage of aeolian deposits gradually decreases towards the west, eventually becoming completely absent west of Duma Point, where the aeolian deposits are replaced with shallow-marine deposits (Figure 5B). It is also evident that the aeolian system becomes generally wetter, moving from the eastern Bartlett Wash towards the west of the study area to the western Duma Point localities, where the dune field deposits pinch out and only sandsheet deposits are observed (Figure 5A).

The coastal plain facies belt corresponds to the Summerville Formation. To the east of Duma Point the coastal plain (COPL) sharply overlays the aeolian dunes (CADF), however, to the west of Duma Point the contact with the underlying tidal deposits (TDMM) west of Duma Point is conformable (Figure 1). The establishment of the coastal plain facies belt in the distal reaches of the continental system indicates a high water table and the deflation of the aeolian dune system. This may show that the coastal plain deposition is a result of the aeolian system directly interacting with the tide-dominated shallow-marine depositional facies belt. Evidence of the interaction between the aeolian system (both coastal

plain and aeolian dune field facies belts) and the tide-dominated shallow-marine is best observed at the facies scale, with relatively constant and similar grain sizes observed in the deflated aeolian system, and the intertidal flat association. This suggests the reworking of aeolian material by tidal currents, creating a boundary that is difficult to distinguish between the two environments, further enhanced by the very low-gradient of the studied system (Wilcox & Currie, 2008; Zuchuat et al., 2019a).

5.2 Temporal evolution of the Curtis-Summerville aeolian to shallow-marine margin

5.2.1 Temporal evolution of terrestrial facies

Four parasequences depicting the evolution of the terrestrial aeolian deposits have been identified, along with three types of aeolian dune cosets and a sandsheet association within the coastal aeolian dune field facies belt, indicating four distinct phases of dune field development and decline (Figure 7. The initial phase of dune field development (phase 1) is evidenced by isolated, small, low-angle climbing sinuous-crested and rare straight-crested dune sets, representing the initial migration of small dunes and dune trains with low sediment availability. The second phase of dune field development (phase 2) is characterised by large, low to moderate-angle climbing sinuous-crested dune sets, representing the development of more mature and larger sinuous-crested dunes. The third phase of dune development (phase 3) is evidenced by low-angle climbing straight-crested dune sets, which often overlie the sinuous-crested dunes. This represents the migration of straight-crested dunes and dune trains, where there has been a possible reduction in sediment availability, and the inability of the basal set surface to be scoured to form pits associated with sinuous-crested dune forms. These cosets of differing dune types are punctuated by large scale bounding surfaces (coset bounding surfaces) that are discordant with underlying set geometries, the succession of preserved dune associations are then overlain by sandsheet associations,

indicating further reduction in sediment availability (phase 4; Figure 6). Each coset shows a typical sediment availability profile, which is evidenced by the upwards changes in the aeolian sediments of the Moab Member. This succession therefore indicates that in the purely aeolian portion of the studied deposits there are four relative water table rises that bound each phase, and which separate the assemblage into four intervals (Figure 6).

The coset bounding surfaces occur over tens of kilometres and can be considered as flooding and deflation surfaces of limited spatial extent. These surfaces could represent supersurfaces (*sensu* Kocurek, 1988). However, to use such a definition in this study would require a wider regional scope, inclusive of Moab Member dune successions to the north and south of the study area. Supersurfaces can represent the shutdown of sediment availability and the deflation of underlying dunes as they become sediment starved (Kocurek, 1988; Kocurek & Havholm, 1993; Mountney, 2006a). The relative sea-level indicators of these surfaces within the aeolian-shallow marine margin environment are largely defined by the presence of rhizoliths (indicating the presence of vegetation) and immature palaeosols. These coset bounding surfaces could therefore represent a more regional surface representing deflation induced by a water table rise.

5.2.2 Temporal evolution of the shallow-marine margin

There are two associations that comprise the shallow marine portion of the Curtis Formation, the more distal subtidal to intertidal flat overlain by the more proximal intertidal to supratidal flat, indicating a progradation associated with a shallowing-upward (Catuneanu, 2006). This progradational pattern occurs twice within the marine margin, and each progradational cycle is bound by a marine flooding surface that punctuates

the marine margin succession. These sequences show characteristics of relative sea-level shallowing between each sequence within the tidally-dominated margin and therefore form a gross progradational geometry indicative of regression.

As the system continued to regress, the shallow marine deposits transition to the overlying coastal plain assemblage of the Summerville Formation. It should be noted that the shallowing observed within the shallow marine sediments is much more gradual, with one environment grading into another, contrary to the sharp bounding surfaces and rapid regression seen within the preserved coastal aeolian succession.

5.3 Transgression and regression in aeolian-marine transitional settings

The Curtis-Summerville system can be subdivided into six spatially and temporally linked parasequences, divided by five time surfaces showing a complete transgressive-regressive cycle, from a maximum transgressive surface datum at the base of the middle Curtis Formation (Figure 6). The nature of transgressions and regressions in such margins is simply documented as the landward or basinward temporal dislocation of depositional environments. This study, however, shows how transgressions and regressions of relative sea-level affect the individual depositional environments and how contemporaneous marginal transitions are influenced by such controls (Figure 8). This section attempts to establish a high-resolution sequence stratigraphic framework for the succession based upon the sequence composition and sequence bounding time surfaces.

Regressional parasequence sets in arid continental margin settings are typically dominated by aeolian dune field expansion. It is well documented that dune field expansion is related to increasing maturity and sediment availability (Mountney, 2006a, 2012). However, when minor transgressions occur, it is interpreted that concurrent water table rises transpire causing minor deflation and stabilisation of the dune field as the

sediment transport availability diminishes (Kocurek & Havholm, 1993). This is observed in discordant contacts and vegetation of supersurfaces. The crucial factor in parasequences preserved within regressional aeolian environments is recovery. In the Moab Member, the phase of growth after the initial supersurface shows increased sediment availability, magnitude and building, forming a progradational parasequence set comprising two parasequences. The first parasequence, associated with the increased sediment availability and the autogenic building of an aeolian system, can be observed at Bartlett Wash and Lone Mesa and is bound by time surface one (T1), a flooding surface (Figure 9). The second parasequence again shows general progradational facies changes with the general expansion of the dune field, and again is bound by a flooding surface (T2) (Figure 8). The upper surface of both these phases is punctuated by rhizoliths and the abrupt nature of the stratal contacts observed at these surfaces indicate relatively high water table conditions. It is therefore likely that these are the result of the above described smaller scale transgressive events that deflate the developing dune field for a period of time.

The T2 flooding surface represents a potentially larger scale surface hereafter referred to as the point of starvation (Figure 9) and marks the transition into the third parasequence which exhibits retrogradation where the back stepping of the aeolian dune field in the Duma Point region and the deposition of intertidal flats in the San Rafael locality is observed. The pattern of dune progression has now changed, such that the dunes decrease in size and complexity up succession, contrary to the underlying units. This suggests that it was a high magnitude regressive event that in fact outpaced sediment supply to the dune field causing the inability of the aeolian system to recover and the degradation of dune forms to a sand sheet. Parasequence four continues this pattern of retrogradation, with the aeolian system retrograding back towards Bartlett Wash and being absent in the Duma Point location. The retrogradation seen between parasequence three and four also shows the emergence of subtidal to intertidal flat associations for the first time in the San Rafael locality. Parasequence five is the final retrogradational package that depicts much of

the same backstepping of facies as the underlying two parasequences (Figure 6). Overlying the retrogradational parasequence set is a distinct facies dislocation that appears across each location and is therefore regionally significant. This is the surface that marks the Curtis-Summerville boundary and is overlain by the coastal plain package (parasequence 6, Figure 9), expanding both landward and seaward with the continued deflation of the dune field and regression of the Curtis Sea.

Consequently, during high-magnitude regressional parasequences the interaction of aeolian systems with tidal margins becomes increasingly deflationary. During these larger scale regressions, sediment supply to the aeolian system becomes increasingly sparse and therefore leads to dune field contraction and deflation from dune field to sand flat. There may therefore be a link between sediment available for aeolian deposition (in this case demonstrated by dune field size) and the pace and scale of regression. In the coastal plain region of the marine margin, sediment availability may increase as the marine system transgresses over the dune field. This is shown in the relative uniformity of grain sizes associated with the sandsheet and supratidal flat sub-environments. This reworking of aeolian deposits lead to very poorly preserved tidal signatures, a pattern that continues into the subtidal zone.

These interpretations allow for the construction of a high-resolution sequence stratigraphic framework for the Curtis-Summerville margin. Although a traditional sequence stratigraphic approach of genetic stratigraphy is not possible for the succession, given the limited temporal nature of the studied interval, a transgressive and regressive sequence framework provides a more feasible context. An initial progradational parasequence set represents the development of the Moab member dunes from the basal surface of the whole transgressive-regressive (T-R) sequence, the Maximum Transgressive Surface, equivalent to the J3 in the study area (Set 1, Figure 9; Zuchuat et al., 2019). The base of the retrogradational parasequence set (Set 2, Figure 9) is marked by a regional surface referred to as the point of starvation; the surface whereby

regression reaches a certain magnitude so that sediment availability is critically limited, and the dune field begins to deflate. The retrogradational parasequence set, is in turn overlain by the strata of a juxtaposed coastal plain sub-environment recorded in the Summerville Formation, indicating a maximum regressive surface and the top surface of the T-R sequence (Figures 7 and 8).

6 Discussion

The aeolian to shallow-marine margin represents a somewhat sheltered environment with tidal currents dominating depositional processes in the shallow sea, efficiently reworking more sporadic bedforms that developed under occasional oscillatory current. Whilst a preserved transition of aeolian dunes into shallow marine deposits is rare (Ahmed Benan & Kocurek, 2000; Rodriguez-Lopez et al., 2012), the interaction between these deposits is obvious and shows a definitive aeolian-marine transition. The pinch out of the aeolian systems onto marginal marine systems has been previously studied, most notably by Rodriguez-Lopez et al. (2012) on the Iberian Desert System, where interaction of aeolian dune-marine deposits and the preservation of aeolian dunes interacting with marine facies at the dune toesets has been described. However, within the Moab-Curtis-Summerville succession no evidence of the interactions described by Rodriguez-Lopez et al. (2012) were found, instead a deflationary sandsheet and a relatively coarse intertidal zone is observed. This may be for several reasons. First, the presence of lagoonal environments, such as the ones observed in the Iberian Desert System and on the Qatar coastline between the main marine system and aeolian system in the zone of interaction, may help to temper the tidal influence of the marine margin impeding the complete deflation of an aeolian system. Moreover, the tidal range of these analogous systems also needs to be considered. The Persian Gulf is a microtidal seaway with a tidal range of *ca* 1-2 m (Lokier et al., 2015) and does not completely deflate the dune field prior to the interaction of the marine system to the subtidal zone. The Sundance Sea that deposited

the Curtis Formation is a mesotidal environment with a tidal range of *ca* 2.6 m (see Zuchuat et al., 2022 and references therein), in addition to being in a state of tidal resonance, which could further enhance the efficiency of tidal current to rework aeolian sand. Further, this high aeolian sand-supply associated with a lack of consolidated mud tends to dissipate the tidal energy less than if consolidated mud occurs in the system, leading to overall stronger tidal currents (Gabioux et al., 2005). Note that the presence of fluid mud at the bottom of the sea would have the opposite effect, enhancing the tidal current even more by lowering the basal shear stress (Gabioux et al., 2005). The presence of an aeolian margin providing clean sand to a neighbouring a tide-dominated sea could therefore help reduce the dissipation of the tidal energy, while the overall physiography of the basin in question remains the primary parameter influencing the ability of tides to propagate in a basin (Collins et al., 2018, 2021; Dean et al., 2019; Zuchuat et al., 2022). The scale of tidal influence can therefore be shown to be a critical factor in the preservation of deflationary aeolian sediments and the outpacing of sediment availability in response to marginal marine influence, and as a result can greatly affect predictions of subsurface architecture and ultimately reservoir characterisation.

The sediment calibre in the tide-dominated shallow-marine sediments and the aeolian dune system are similar. This is due to the reworking of sediment during transgression. The reworking of aeolian deposits provides a relatively high sediment supply to the marine margin during transgression. This, in combination with the relative deflation of the aeolian dune field in the seaward direction, can make the identification of aeolian-marine stratigraphic surfaces somewhat indecipherable, especially if tidal currents are too low to generate new bedforms. Sediment supply to the aeolian system, created by the availability of mobile sediment and influenced by water table levels, can therefore be influenced, in turn, by the rate in which that water table changes. If the rate of water table rise (as affected by relative sea level) is of a large-enough magnitude and sufficient rate, it may impede the recovery of an aeolian dune field during subsequent regression. The Moab Member-to-Summerville boundary

exhibits a change from deflationary dune field to a widespread supratidal flat (Figure 9). The supratidal flat strata expands both seaward and landward to overlay a subtidal to intertidal flat association in the San Rafael Swell locality and are therefore considered to be the result of a widespread regression. This defined regressive depositional environment demonstrates the second critical factor in the characteristics of an aeolian marine margin. Where normal regression occurs the Moab Member dune field can recover from small-scale reductions in sediment availability, however, as discussed if the regression reaches sufficient magnitude and develops rapidly then the reduction in sediment availability outpaces erg expansion and therefore the environment transitions away from aeolian dune growth, into an extensive coastal plain.

7 Conclusion

This study has revealed there are two critical influences on sediment deposition and preservation upon an aeolian-marine margin. First, whether a system is transgressive or regressive, and second, the scale of tidal influence. In the case of the Jurassic Curtis-Summerville succession of central Utah, the dune field has been documented to respond to changes in relative sea level by expanding within regressional settings and deflating within transgressional ones. Whilst this relationship is intuitive, added complexities change the characteristics of this environment. These complexities were exacerbated by the direct contact between the dry aeolian dune field and the tide-dominated shallow-marine margin, in addition to the amplified tidal forces caused by tidal resonance within the Curtis Sea basin. When compared with analogues such as the Cretaceous Iberian Desert System and the modern-day Qatar coast, this raises important questions as to the tidal range necessary to completely deflate the dune-field, as seen here, or simply to affect dune morphologies, as seen in modern environments.

These complexities make identifying sequence stratigraphical boundaries and correlating across the margin somewhat challenging. This has been overcome by attributing the deflationary surfaces, linked with changes in relative sea level, to sequence boundaries, and documenting the transition between depositional environments at a T-R sequence scale.

Following the regional transgression recorded at base of the Moab Member and the middle Curtis Formation the dune field expanded preserving two cosets increasing in sinuosity and bedform size up succession. Following this, the system continued to regress, preserving three further dune cosets separated by bounding surfaces. Each of these surfaces marks a period of small-scale transgression, shutting down sediment availability and causing deflation. After each of these surfaces the ability of the dune field to recover decreased, until eventually, the sediment starved coastal plain assemblage dominated. Despite this pattern of regression promoting dune growth, punctuated by deflation caused by local transgression, this study notes the point of starvation is the point at which regression outpaces sediment supply, starving the dune field and eventually promoting the takeover of coastal plain sediments. It is therefore suggested that whilst regression promotes dune growth in most circumstances, beyond a point of critical regression, sediment availability and consequently dune growth are hampered causing a shutdown of aeolian processes within this shallow marine margin environment.

Using these sequences allows for the correlation of flooding events between tide-dominated shallow-marine sediments and dry aeolian successions. This has wider consequences for placing these deposits within a global timescale and provides a hypothesis for allocyclic controls on the depositional environment driven by the well-documented climate changes throughout the Oxfordian. Whilst further work is required to secure an age constraint on these deposits, this study has been able to identify small-scale and large-scale interactions upon an aeolian-marine margin,

document changes in dune geometries with proximity to said margin and describe margin changes relative to the sequence stratigraphy of the basin.

Acknowledgements

David Hodgetts of the University of Manchester is thanked for the use of VRGS software. Brock Arvesen is thanked for providing valuable field support. The authors declare that they have no conflict of interests. Gary Kocurek, Juan Pedro Rodríguez-López and Nigel Mountney are warmly acknowledged for their comments that helped improve the quality of this manuscript. This paper is published by permission of the Executive Director of the British Geological Survey (UKRI).

Author Contributions

SC: conceptualisation (lead), data curation (lead), formal analysis (lead), investigation (equal), methodology (equal), project administration (lead), visualisation (lead), writing original draft (lead), writing- review & editing (lead) **RPP**: conceptualisation (supporting), data curation (supporting), investigation (equal), methodology (equal), validation (lead), supervision (lead), writing original draft (supporting), writing- review & editing (supporting) **CLP:** conceptualisation (supporting), data curation (supporting), validation (supporting), writing original draft (supporting), writing-review & editing (supporting) **VZ**: conceptualisation (supporting), writing-review & editing (supporting) **TJD**: writing- review & editing (supporting) **AJM**: writing original draft (supporting), visualisation (supporting), writing-review and editing (supporting) **SMC**: funding acquisition (lead), writing-review & editing (supporting)

Data Availability Statement

The data that support the findings of this study are available from the corresponding author upon reasonable request.

Table Captions

Table 1 – Facies descriptions and interpretations for the Curtis-Summerville successions exposed in the study area.

Table 2 – Facies association descriptions and interpretations for the Curtis-Summerville successions exposed in the study area.

Figure Captions

Figure 1: (A) Map of the study area, documenting the localities taken across the study area. Locations where a drone survey was conducted is indicated with a drone symbol. Top right contains a map of the United States of America, the state of Utah and the study area highlighted within. (B) Schematic lithostratigraphic column showing correlation between late Triassic and Jurassic deposits between Central Utah and Northern New Mexico (after, Zuchuat et al., 2019). (C) Logs and locations taken across the study area. (D) Representative field photograph showing the relationship between formations analysed by this study.

Figure 2: (A) Map of localities where sedimentary logging was conducted, transect line is marked. (B) Sedimentary logs at each locality, coloured by facies with the associations and assemblages represented down the left side of each log. Sedimentary structures of note are shown on the right-hand side. Where outcrops were inaccessible, the depth has been estimated and marked with a cross.

Figure 3: (A) Aeolian dune succession at 2a: Lone Mesa showing a vertical proximal to distal aeolian trend from low-angle climbing straight-crested dune sets (a) to small low-angle climbing sinuous-crested dune sets (b). The top-most stratigraphic surface is irregular, showing palaeo-relief of preserved dune forms. (B) Small low-angle climbing sinuous-crested dune sets (b) with indications of rooting (c) at 1: Bartlett Wash. (C) Large low-moderate angle climbing sinuous crested dunes (d) overlain by smaller low-angle climbing straight crested dunes (a) at 3: Duma Point Transition 3. (D) Low-angle straight-crested dunes (a) grading into structureless sand sheet facies (e) at 2a: Lone Mesa.

Figure 4: (A) Wavy ripple laminated sandstones at 5: San Rafael Swell, note the round-crested ripples and internal lamination indicating relatively deep water with a high sediment load. (B) Flaser bedded sandstones at 5: San Rafael Swell, cavities in the ripple peaks are the result of erosion of finer-grained material, a clear indicator of a tidal environment. (C) Ferric gleysol preserved at 3: Duma Point Transition 3, vertical burrows and evidence of rooting are visible. (D) Vein and laminar beds of gypsum within the parallel laminated gypsisol facies at 5: San Rafael Swell, note the

vein gypsum bisects the bedded gypsum and is therefore likely to be a secondary feature. (E) Herringbone cross-stratified sandstone facies at 5: San Rafael Swell, the bidirectional preserved ripples are a clear indicator of a tidal environment. (F) Wavy bedded sandstone at 4: Duma Point Transition 3, round-crests and some immature ripple development indicates very shallow water with low sediment supply.

Figure 5: (A) Schematic diagram showing the spatial transition between associations east to west across the study area. Sinuous crested dunes transition into smaller sinuous crested and straight crested dunes before deflating into a sandsheet. The supratidal flat expands both landward and seaward grading into an intertidal flat, and once the water depth becomes significant enough, a subtidal- intertidal flat. (B) Relative proportions of each association at each locality.

Figure 6: W-E correlated panel from the tide-dominated shallow-marine margin at 5: San Rafael Swell to the aeolian dune successions at 1: Bartlett Wash. The logs have been coloured by facies; correlation has been made by association. Sedimentary structures of note are shown on the right-hand side of each log. Where outcrops were inaccessible, the depth has been estimated and marked with a cross. Note the log below the MTS has been greyed out, it is important to observe the underlying lower Curtis sediments, however, they are not the subject of this study and therefore have not been discussed.

Figure 7: Phases of dune growth at each locality, Phase 1 is represented in blue, Phase 2 in green and Phase 3 in yellow. Underlying and overlying deposits of Entrada Formation and Coastal Plain assemblage are marked accordingly. (A) Three phases of dune growth at 1: Bartlett Wash. (B) Three phases of dune growth at 2b: Dubinky Well, note the relative thickness of phase 1 is decreased, however, the thickness of phase 2 has increased compared with 1: Bartlett Wash. (C) Phases of dune growth at 3: Duma Point Transition 1, note that this is the closest locality to the margin and here only one phase of dune expansion is evident.

Figure 8: Depositional environment models for the temporal translation of assemblages. T1 represents the regression of the Curtis Sea and the development of the Moab member dune field following the major transgressive event preserved within the J3. T2 marks continued development of the dune field, with dune size and complexity increasing with continued fall in sea level. T3 represents the point of starvation, after which the dune field begins to deflate and the coastal plain begins to expand both landward and seaward. T4 shows the inability of the dune field to recover from this high-magnitude, rapid regression, shutting down sediment supply and preserving small dune forms and sand sheets. T5 marks the final shut down of all aeolian processes in the east of the study area and the complete takeover of the coastal plain sediments of the Summerville Formation.

Figure 9: Cyclicity and sequence stratigraphy within the studied Curtis-Summerville formations. The left-hand side separates the interpreted units into parasequences. (A) Broad scale transgressive-regressive sequence from the maximum transgressive surface of the J-3 to the maximum transgressive surface within the Summerville. Red represents regression, blue represents transgression. (B) Smaller scale transgressive and regressive events. Red represents regression, blue represents transgression. (C - E) Schematic logs of the associations identified from the distal setting with tide-dominated shallow-marine deposits, through to the proximal setting with continental aeolian deposits. (F) Regional sea-level fluctuation associated with the broad-scale transgressive-regressive sequence. (G) Local scale sea-level fluctuations associated with the smaller-

scale transgressive and regressive events. (H) Interpreted sedimentation rate curve across the margin, note the rate of sedimentation increases to the point of starvation and then decreases towards the maximum regressive surface.

References

Ahmed Benan, C.A. and Kocurek, G., (2000). Catastrophic flooding of an aeolian dune field: Jurassic Entrada and Todilto formations, Ghost Ranch, New Mexico, USA. Sedimentology, 47(6), pp.1069-1080. https://doi.org/10.1046/j.1365-3091.2000.00341.x

Allen, P.A., 1984. Reconstruction of ancient sea conditions with an example from the Swiss Molasse. *Marine Geology*, 60(1-4), pp.455-473.

Al-Masrahy, M.A. and Mountney, N.P., 2015. A classification scheme for fluvial–aeolian system interaction in desert-margin settings. *Aeolian Research*, 17, pp.67-88. https://doi.org/10.1016/j.aeolia.2015.01.010

Anderson, O.J., and Lucas, S.G. (1994). Middle Jurassic stratigraphy, sedimentation and paleogeography in the southern Colorado Plateau and southern High Plains. In: Caputo, M.V., Peterson, J.A., and Franczyk, K.J. (Eds.), Mesozoic Systems of the Rocky Mountain Region, USA, SEPM, Rocky Mountain Section, 299-314

Anderson, T.H. (2015). Jurassic (170–150 Ma) basins: The tracks of a continental-scale fault, the Mexico–Alaska mega shear, from the Gulf of Mexico to Alaska. In Anderson, T.H., Didenko, A.N., Johnson, C.L., Khanchuk, A.I., and MacDonald, J.H. (Eds.), Late Jurassic margin of Laurasia: a record of faulting accommodating plate rotation, Geological Society of America, Special Paper 513, 107-188. https://doi.org/10.1130/2015.2513(03)

Andeskie, A. S., Benison, K. C., Eichenlaub, L. A., & Raine, R. (2018). Acid-saline-lake systems of the Triassic Mercia Mudstone Group, County Antrim, Northern Ireland. Journal of Sedimentary Research, 88(3), 385-398. https://doi.org/10.2110/jsr.2018.14

Baas, J. H., Best, J. L., & Peakall, J. (2016). Predicting bedforms and primary current stratification in cohesive mixtures of mud and sand. Journal of the Geological Society, 173(1), 12-45. https://doi.org/10.1144/jgs2015-024

Bagnold, R. A., (1941), The physics of blown sand and desert dunes. New York (Morrow), 265 pp. https://doi.org/10.1177%2F030913339401800105

Banham, S.G., S. Gupta, S.D., Rubin, D., J. Watkins, K.S. Edgett, D. Sumner, J. Grotzinger, K. Lewis, L. Edgar, K. Stack, R. Barnes, J.F. Bell III, M. Day, R. Ewing, M.G. Lapôtre, F. Rivera-Hernandez, A.R. Vasavada, (2018). Ancient Martian aeolian processes and palaeomorphology reconstructed

from the Stimson formation on the lower slope of Aeolis Mons, Gale crater, Mars. Sedimentology **65**, 993–1042. https://doi.org/10.1111/sed.12469

Bemis, S.P., Micklethwaite, S., Turner, D., James, M.R., Akciz, S., Thiele, S.T. and Bangash, H.A., (2014). Ground-based and UAV-Based photogrammetry: A multi-scale, high-resolution mapping tool for structural geology and paleoseismology. Journal of Structural Geology, 69, pp.163-178. https://doi.org/10.1016/j.jsg.2014.10.007

Bjerrum, C.J. and Dorsey, R.J., (1995). Tectonic controls on deposition of Middle Jurassic strata in a retroarc foreland basin, Utah-Idaho trough, western interior, United States. Tectonics, 14(4), pp.962-978. https://doi.org/10.1029/95TC01448

Bradley, G. M., Redfern, J., Hodgetts, D., George, A. D., & Wach, G. D. (2018). The applicability of modern tidal analogues to pre-vegetation paralic depositional models. Sedimentology, 65(6), 2171-2201. https://doi.org/10.1111/sed.12461

Brenner, R.L., and Peterson, J.A. (1994). Jurassic sedimentary history of the northern portion of the Western Interior Seaway, USA. In: Caputo, M.V., Peterson, J.A., and Franczyk, K.J. (Eds.), Mesozoic Systems of the Rocky Mountain Region, USA, SEPM, Rocky Mountain Section, 233-272.

Bullard, J.E., (1997). A note on the use of the" Fryberger method" for evaluating potential sand transport by wind. Journal of Sedimentary Research, 67(3), pp.499-501. https://doi.org/10.1306/D42685A9-2B26-11D7-8648000102C1865D

Buol, S. W., and Eswaran, H. (1999). Oxisols. Advances in Agronomy. **68**, 151–195. https://doi.org/10.1016/S0065-2113(08)60845-7

Campos-Soto, S., Benito, M.I., Mountney, N.P., Plink-Björklund, P., Quijada, I.E., Suarez-Gonzalez, P. and Cobos, A., 2022. Where humid and arid meet: Sedimentology of coastal siliciclastic successions deposited in apparently contrasting climates. Sedimentology, 69(3), pp.975-1027.

Catuneanu, O., (2006). Principles of Sequence Stratigraphy. Elsevier, Amsterdam, pp. 375. https://doi.org/10.1017/S0016756807003627

Caputo M.V., and Pryor W.A. (1991). Middle Jurassic tide- and wave-influenced coastal facies and paleogeography, upper San Rafael Group, east-central Utah. In: T.C. Chidsey (Ed.), Geology of East-Central Utah, Utah Geological Association, Salt Lake City, 9-27.

Carr-Crabaugh, M., and Kocurek, G. (1998). Continental sequence stratigraphy of a wet eolian system: a key to relative sea-level change. In: Stanley, K.W., and McCabe, P.J. (Eds.), Relative Role of Eustasy, Climate, and Tectonics in Continental Rocks, SEPM, Special Publication 59, 213-228. https://doi.org/10.2110/pec.98.59.0212

Chan, M.A., 1989. Erg margin of the Permian white rim sandstone, SE Utah. *Sedimentology*, *36*(2), pp.235-251.

Chandler, F.W., Sullivan, R.W. and Currie, K.L., (1987). The age of the Springdale Group, western Newfoundland, and correlative rocks—evidence for a Llandovery overlap assemblage in the Canadian Appalachians. Earth and Environmental Science Transactions of The Royal Society of Edinburgh, 78(1), pp.41-49. https://doi.org/10.1017/S0263593300010944

Chandler, M.A., Kocurek, G., Goggin, D.J. and Lake, L.W., (1989). Effects of stratigraphic heterogeneity on permeability in eolian sandstone sequence, Page Sandstone, northern Arizona. AAPG bulletin, 73(5), pp.658-668. https://doi.org/10.1306/44B4A249-170A-11D7-8645000102C1865D

Chedburn, L., Underhill, J.R., Head, S. and Jamieson, R., 2022. The critical evaluation of carbon dioxide subsurface storage sites: Geological challenges in the depleted fields of Liverpool Bay. *AAPG Bulletin*, *106*(9), pp.1753-1789. https://doi.org/10.1306/07062221120

Clemmensen, L. B., & Blakey, R. C. (1989). Erg deposits in the Lower Jurassic Wingate Sandstone, northeastern Arizona: oblique dune sedimentation. Sedimentology, 36(3), 449-470. https://doi.org/10.1111/j.1365-3091.1989.tb00619.x

Collins, D.S., Avdis, A., Allison, P.A., Johnson, H.D., Hill, J. and Piggott, M.D., (2018). Controls on tidal sedimentation and preservation: Insights from numerical tidal modelling in the Late Oligocene–Miocene South China Sea, Southeast Asia. Sedimentology, 65(7), pp.2468-2505. https://doi.org/10.1111/sed.12474

Collins, D. S., Avdis, A., Wells, M. R., Dean, C. D., Mitchell, A. J., Allison, P. A., ... and Piggott, M. D. (2021). Prediction of shoreline–shelf depositional process regime guided by palaeotidal modelling. Earth-Science Reviews, 223, 103827. https://doi.org/10.1016/j.earscirev.2021.103827

Collinson, J., and Mountney, N (2019) Sedimentary Structures. Dunedin Academic Press Ltd (Fourth Edition) 340 pp

Cosgrove, G. I. E., Colombera, L., & Mountney, N. P. (2022). The role of subsidence and accommodation generation in controlling the nature of the aeolian stratigraphic record. Journal of the Geological Society, 179 (1) https://doi.org/10.1144/jgs2021-042

Crabaugh, M., and Kocurek, G. (1993). Entrada Sandstone: an example of a wet aeolian system. In: Pye, K. (Ed.), The Dynamics and Environmental Context of Aeolian Sedimentary Systems, Geological Society of London, Special Publication, 72, 103-126. https://doi.org/10.1144/GSL.SP.1993.072.01.11

Danise, S., and Holland, S.M. (2017). Faunal response to sea-level and climate change in a short-lived seaway: Jurassic of the Western Interior, USA. Palaeontology, 60(2), 213-232. https://doi.org/10.1111/pala.12278

Danise, S., and Holland, S.M. (2018). A sequence stratigraphic framework for the Middle to Late Jurassic of the Sundance Seaway, Wyoming: implications for correlation, basin evolution, and climate change. The Journal of Geology, 126(4), 371-405. https://doi.org/10.1086/697692

Danise, S., Price, G.D., Alberti, M., and Holland, S.M. (2020). Isotopic evidence for partial geochemical decoupling between a Jurassic epicontinental sea and the open ocean. Gondwana Research, 82, 97-107. https://doi.org/10.1016/j.gr.2019.12.011

Dean, C. D., Collins, D. S., van Cappelle, M., Avdis, A., and Hampson, G. J. (2019). Regional-scale paleobathymetry controlled location, but not magnitude, of tidal dynamics in the Late Cretaceous Western Interior Seaway, USA. Geology, 47(11), 1083-1087. https://doi.org/10.1130/G46624.1

Desjardins, P.R., Buatois, L.A., Pratt, B.R. and Mangano, M.G., (2012). Forced regressive tidal flats: response to falling sea level in tide-dominated settings. Journal of Sedimentary Research, 82(3), pp.149-162. https://doi.org/10.2110/jsr.2012.18

Doelling, H.H., (2001), Geologic map of the Moab and eastern part of the San Rafael Desert 30' x 60' quadrangles, Grand and Emery Counties, Utah, and Mesa County, Colorado: Utah Geological Survey Map 180, scale 1:100,000 (Digital map with GIS data released as Map 180DM in 2002).

Doelling, H.H., (2002), Geological map of the Moab and eastern part of the San Rafael Desert 300 9 600 quadrangles, Grand and Emery counties, Utah, and Mesa County, Colorado. Utah Geological Survey

Doelling, H.H., Sprinkel, D.A., Kowallis, B.J., and Kuehne, P.A. (2013). Temple Cap and Carmel Formations in the Henry Mountains Basin, Wayne and Garfield Counties, Utah. The San Rafael Swell and Henry Mountains Basin—geologic centerpiece of Utah: Utah Geological Association Publication, 42, 279-318

Doelling, H.H., Kuehne, P.A., Willis, G.C. and Ehler, J.B., (2015). Geologic map of the San Rafael Desert 30 x 60-minute quadrangle. Emery and Grand Counties, Utah: Salt Lake City, Utah, Utah Geological Survey, scale, 1(62,500), p.3.

Ewing, R.C. and Kocurek, G.A., (2010). Aeolian dune interactions and dune-field pattern formation: White Sands Dune Field, New Mexico. Sedimentology, 57(5), pp.1199-1219. https://doi.org/10.1111/j.1365-3091.2009.01143.x

Flemming, B.W. (2011). Geology, morphology, and sedimentology of estuaries and coasts. In: Treatise on Estuarine and Coastal Science, E. Wolanski and D. McLusky (eds). Waltham, USA: Academic Press, 7–38. http://dx.doi.org/10.1016/B978-0-12-374711-2.00302-8

Fryberger, S.G., 1984. The Permian Upper Minnelusa Formation, Wyoming: Ancient example of an offshore-prograding eolian sand sea with geomorphic facies, and system-boundary traps for petroleum.

Fryberger, S.G. and Schenk, C.J., (1988). Pin stripe lamination: a distinctive feature of modern and ancient eolian sediments. Sedimentary Geology, 55(1-2), pp.1-15. https://doi.org/10.1016/0037-0738(88)90087-5

Fossen, H., 2010. Deformation bands formed during soft-sediment deformation: observations from SE Utah. *Marine and Petroleum Geology*, *27*(1), pp.215-222.

Gabioux, M., Vinzon, S. B., and Paiva, A. M. (2005). Tidal propagation over fluid mud layers on the Amazon shelf. Continental Shelf Research, 25(1), 113-125. https://doi.org/10.1016/j.csr.2004.09.001

Gilluly, J., and Reeside, J.B. Jr. (1928). Sedimentary rocks of the San Rafael Swell and some adjacent areas in eastern Utah. U.S. Geological Survey, Professional Paper 150-D, 61-110. https://doi.org/10.3133/pp150D

Gradziński, R. and Uchman, A., (1994). Trace fossils from interdune deposits—an example from the Lower Triassic aeolian Tumlin Sandstone, central Poland. Palaeogeography, Palaeoclimatology, Palaeoecology, 108(1-2), pp.121-138. https://doi.org/10.1016/0031-0182(94)90025-6

Gross, E.C., Carr, M. and Jobe, Z.R., 2022. Three-dimensional bounding surface architecture and lateral facies heterogeneity of a wet aeolian system: Entrada Sandstone, Utah. Sedimentology.

Hawley, N., 1981. Flume experiments on the origin of flaser bedding. *Sedimentology*, *28*(5), pp.699-712. https://doi.org/10.1111/j.1365-3091.1981.tb01930.x

Henares, S., Caracciolo, L., Cultrone, G., Fernández, J. and Viseras, C., (2014). The role of diagenesis and depositional facies on pore system evolution in a Triassic outcrop analogue (SE Spain). Marine and Petroleum Geology, 51, pp.136-151. https://doi.org/10.1016/j.marpetgeo.2013.12.004

Hicks, T.C., 2011. Facies Analysis and Reservoir Characterization of Subtidal, Intertidal, and Supratidal Zones of the Mudstone-rich Entrada Sandstone, South-Central Utah. Brigham Young University.

Hintze, L. and Kowallis, B., (2009). Geological history of Utah. Brigham Young University Geology Studies.

Hodgetts, D., Gawthorpe, R.L., Wilson, P., and Rarity, F (2007) Integrating digital and traditional field techniques using virtual reality geological studio (VRGS), 69th European Association of Geoscientists and Engineers Conference and Exhibition, incorporating SPE EUROPEC 2007, pp. 83-87 https://doi.org/10.3997/2214-4609.201401718

Howell, J. A., Chmielewska, M., Lewis, C., Buckley, S., Naumann, N., and Pugsley, J. (2021). Acquisition of Data for Building Photogrammetric Virtual Outcrop Models for the Geosciences using Remotely Piloted Vehicles (RPVs). EarthArXiv https://doi.org/10.31223/X54914

Hunter, R.E., (1977). Basic types of stratification in small eolian dunes. Sedimentology, 24(3), pp.361-387. https://doi.org/10.1111/j.1365-3091.1977.tb00128.x

Huntoon, J.E. and Chan, M.A., 1987. Marine origin of paleotopographic relief on eolian White Rim Sandstone (Permian), Elaterite basin, Utah. *AAPG Bulletin*, *71*(9), pp.1035-1045.

Imlay, R.W. (1952). Correlation of the Jurassic formations of North America, exclusive of Canada. Geological Society of America Bulletin, 63(9), 953-992. https://doi.org/10.1130/0016-7606(1952)63[953:COTJFO]2.0.CO;2

Imlay, R.W. (1980). Jurassic Paleobiogeography of the Conterminous United States in its Continental Setting. U.S. Geological Survey, Professional Paper, 1062, 134 pp. https://doi.org/10.3133/pp1062

Jerram, D.A., Mountney, N.P., Howell, J.A., Long, D. and Stollhofen, H., (2000). Death of a sand sea: an active aeolian erg systematically buried by the Etendeka flood basalts of NW Namibia. Journal of the Geological Society, 157(3), pp.513-516. https://doi.org/10.1144/jgs.157.3.513

Jennings III, G.R., 2014. Facies analysis, sequence stratigraphy and paleogeography of the Middle Jurassic (Callovian) Entrada Sandstone: traps, tectonics, and analog. Brigham Young University.

Jordán, M. M., Navarro-Pedreno, J., García-Sánchez, E., Mateu, J., & Juan, P. (2004). Spatial dynamics of soil salinity under arid and semi-arid conditions: geological and environmental implications. Environmental geology, 45(4), 448-456. https://doi.org/10.1007/s00254-003-0894-y

Jordan, O.D. and Mountney, N.P., 2010. Styles of interaction between aeolian, fluvial and shallow marine environments in the Pennsylvanian to Permian lower Cutler beds, south-east Utah, USA. *Sedimentology*, *57*(5), pp.1357-1385.

Jordan, O.D. and Mountney, N.P., 2012. Sequence stratigraphic evolution and cyclicity of an ancient coastal desert system: the Pennsylvanian-Permian lower Cutler beds, Paradox Basin, Utah, USA. Journal of Sedimentary Research, 82, 755-780. 10.2110/jsr.2012.54

Kemp, J., Pietsch, T., Gontz, A. and Olley, J., 2017. Lacustrine-fluvial interactions in Australia's Riverine Plains. *Quaternary Science Reviews*, 166, pp.352-362. https://doi.org/10.1016/j.quascirev.2017.02.015

Kocurek, G., (1988). First-order and super bounding surfaces in eolian sequences—bounding surfaces revisited. Sedimentary Geology, 56(1-4), pp.193-206. https://doi.org/10.1016/0037-0738(88)90054-1

Kocurek, G., (1991). Interpretation of ancient eolian sand dunes. Annual review of Earth and planetary sciences, 19(1), pp.43-75. https://doi.org/10.1146/annurev.ea.19.050191.000355

Kocurek, G. and Nielson, J., (1986). Conditions favourable for the formation of warm-climate aeolian sand sheets. Sedimentology, 33(6), pp.795-816. https://doi.org/10.1111/j.1365-3091.1986.tb00983.x

Kocurek, G., & Havholm, K. (1993). Eolian sequence stratigraphy – A conceptual framework. In: P. Weimer, & H. Posamentier (Eds.), *Siliciclastic sequence stratigraphy* (pp. 393–409). American Association of Petroleum Geologists Memoir. https://doi.org/10.1306/M58581C16

Kocurek, G. and Lancaster, N., 1999. Aeolian system sediment state: theory and Mojave Desert Kelso dune field example. *Sedimentology*, *46*(3), pp.505-515.

Kocurek, G., Robinson, N.I. and Sharp, J.M. Jr., 2001. The response of the water table in coastal aeolian systems to changes in sea level. Sedimentary Geology, 139, 1-13. https://doi.org/10.1016/S0037-0738(00)00137-8

Kok, J.F., Parteli, E.J., Michaels, T.I. and Karam, D.B., (2012). The physics of wind-blown sand and dust. Reports on progress in Physics, 75(10), p.106901. https://doi.org/10.1088/0034-4885/75/10/106901

Kumar, N. and Sanders, J.E., (1976). Characteristics of shoreface storm deposits; modern and ancient examples. Journal of Sedimentary Research, 46(1), pp.145-162. https://doi.org/10.1306/212F6EDD-2B24-11D7-8648000102C1865D

Kreisa, R.D. and Moila, R.J., (1986). Sigmoidal tidal bundles and other tide-generated sedimentary structures of the Curtis Formation, Utah. Geological Society of America Bulletin, 97(4), pp.381-387. https://doi.org/10.1130/0016-7606(1986)97%3C381:STBAOT%3E2.0.CO;2

Kvale, E.P., 2012. Tidal constituents of modern and ancient tidal rhythmites: criteria for recognition and analyses. In *Principles of tidal sedimentology* (pp. 1-17). Springer, Dordrecht.

Langford, R.P., 1989. Fluvial-aeolian interactions: Part I, modern systems. *Sedimentology,* 36(6), pp.1023-1035. https://doi.org/10.1111/j.1365-3091.1989.tb01540.x

Lizzoli, S., Raigemborn, M.S. and Varela, A.N., (2021). Controls of pedogenesis in a fluvial-eolian succession of Cenomanian age in northern Patagonia. Palaeogeography, Palaeoclimatology, Palaeoecology, 577, p.110549. https://doi.org/10.1016/j.palaeo.2021.110549

Lockley, M., (2021a). Integration of tetrapod ichnofaunas and coastal dynamics for paleocommunity reconstruction in the Curtis and Summerville formations (Jurassic), eastern Utah. Historical Biology, pp.1-18. https://doi.org/10.1080/08912963.2021.1946531

Lockley, M., (2021b). The distribution of theropod-dominated ichnofaunas in the Moab Megatracksite area, Utah: implications for Late Jurassic palaeobiology along an arid coast. Historical Biology, pp.1-35. https://doi.org/10.1080/08912963.2021.1975279

Lokier, S.W., Bateman, M.D., Larkin, N.R., Rye, P. and Stewart, J.R., (2015). Late Quaternary sea-level changes of the Persian Gulf. Quaternary Research, 84(1), pp.69-81. https://doi.org/10.1016/j.yqres.2015.04.007

Loope, D.B., 1981. Products and Processes of Ancient Arid Coastline: Lower Cutler Group (Permian), Southeastern Utah. *AAPG Bulletin*, *65*(5), pp.950-951.

Loope, D.B., (1988). Rhizoliths in ancient eolianites. Sedimentary Geology, 56(1-4), pp.301-314. https://doi.org/10.1016/0037-0738(88)90058-9

Lucas, S.G., Anderson, O.J. and Kues, B.S., (1997). The Jurassic San Rafael Group, Four Corners region. In Mesozoic geology and paleontology of the Four Corners region: New Mexico Geological Society, 48th Annual Fall Field Conference Guidebook (pp. 115-132). https://doi.org/10.56577/FFC-48.115

Lucas, S.G. and Anderson, O.J., (1998) Jurassic stratigraphy and correlation in New Mexico. New Mexico Geology, 20(4), pp.97-104.

Lucas, S., (2014). Lithostratigraphy of the Jurassic San Rafael Group from Bluff to the Abajo Mountains, southeastern Utah: Stratigraphic relationships of the Bluff Sandstone. Volumina Jurassica, 12(2). http://dx.doi.org/10.5604/17313708+.1130128

Mack, G. H., James, W. C., andMonger, H. C. (1993). Classification of paleosols. Geological society of America bulletin, 105(2), 129-136.https://doi.org/10.1130/0016-7606(1993)105%3C0129:COP%3E2.3.CO;2

Maidment, S.C. and Muxworthy, A., (2019). A chronostratigraphic framework for the Upper Jurassic Morrison Formation, western USA. Journal of Sedimentary Research, 89(10), pp.1017-1038. https://doi.org/10.2110/jsr.2019.54

Martel, A.T. and Gibling, M.R. (1991) Wave-dominated lacustrine facies and tectonically controlled cyclicity in the Lower Carboniferous Horton Bluff Formation, Nova Scotia, Canada. In: Lacustrine Facies Analysis (Eds. Anadon, P., Cabera, L. and Kelts, K.), International Association of Sedimentologists, Special Publication, 13, 223–243. https://doi.org/10.1002/9781444303919.ch11

Martinius, A. W., and Gowland, S. (2011). Tide-influenced fluvial bedforms and tidal bore deposits (late Jurassic Lourinhã Formation, Lusitanian Basin, Western Portugal). Sedimentology, 58(1), 285-324. https://doi.org/10.1111/j.1365-3091.2010.01185.x

McCrory, V.L. and Walker, R.G., (1986). A storm and tidally-influenced prograding shoreline—Upper Cretaceous Milk River Formation of Southern Alberta, Canada. Sedimentology, 33(1), pp.47-60. https://doi.org/10.1111/j.1365-3091.1986.tb00744.x

McKee, E.D. and Weir, G.W., 1953. Terminology for stratification and cross-stratification in sedimentary rocks. *Geological Society of America Bulletin*, *64*(4), pp.381-390. https://doi.org/10.1130/0016-7606(1953)64[381:TFSACI]2.0.CO;2

Mesquita, Á.F., Basilici, G., Soares, M.V.T. and Garcia, R.G.V., 2021. Morphology, accumulation and preservation of draa systems in a Precambrian erg (Galho do Miguel Formation, SE Brazil). Sedimentary Geology, 412, p.105807. https://doi.org/10.1016/j.sedgeo.2020.105807

Milroy, P., Wright, V.P. and Simms, M.J., (2019). Dryland continental mudstones: Deciphering environmental changes in problematic mudstones from the Upper Triassic (Carnian to Norian) Mercia Mudstone Group, south-west Britain. Sedimentology, 66(7), pp.2557-2589. https://doi.org/10.1111/sed.12626

Mountney, N.P. (2006a) Periodic accumulation and destruction of aeolian erg sequences: The Cedar Mesa Sandstone, White Canyon, southern Utah. Sedimentology, 53, 789-823. https://doi.org/10.1111/j.1365-3091.2006.00793.x

Mountney, N.P. (2006b) Eolian Facies Models. In: Facies Models Revisited (Eds H. Posamentier and R.G. Walker). SEPM Mem., 84, 19- 83. https://doi.org/10.2110/pec.06.84.0019

Mountney, N.P., (2012). A stratigraphic model to account for complexity in aeolian dune and interdune successions. Sedimentology, 59(3), pp.964-989. https://doi.org/10.1111/j.1365-3091.2011.01287.x

Mountney, N.P. and Jagger, A., (2004). Stratigraphic evolution of an aeolian erg margin system: the Permian Cedar Mesa Sandstone, SE Utah, USA. Sedimentology, 51(4), pp.713-743. https://doi.org/10.1111/j.1365-3091.2004.00646.x

Mountney, N.P. and Thompson, D.B., (2002). Stratigraphic evolution and preservation of aeolian dune and damp/wet interdune strata: an example from the Triassic Helsby Sandstone Formation, Cheshire Basin, UK. Sedimentology, 49(4), pp.805-833. https://doi.org/10.1046/j.1365-3091.2002.00472.x

Olivero, E. B., Ponce, J. J., & Martinioni, D. R. (2008). Sedimentology and architecture of sharp-based tidal sandstones in the upper Marambio Group, Maastrichtian of Antarctica. Sedimentary Geology, 210(1-2), 11-26. https://doi.org/10.1016/j.sedgeo.2008.07.003

Peterson, F., (1988). Pennsylvanian to Jurassic eolian transportation systems in the western United States. Sedimentary Geology, 56(1-4), pp.207-260. https://doi.org/10.1016/0037-0738(88)90055-3

Peterson, F. (1994). Sand dunes, sabkhas, streams, and shallow seas: Jurassic paleography in the southern part of the Western Interior Basin. In: Caputo, M.V., Peterson, J.A., and Franczyk, K.J. (Eds.), Mesozoic Systems of the Rocky Mountain Region, USA, SEPM, Rocky Mountain Section, 233-272

Peterson, F., and Pipiringos, G.N., (1979), Stratigraphic relations of the Navajo Sandstone to Middle Jurassic formations, southern Utah and northern Arizona: U.S. Geological Survey Professional Paper 1035-B, p. B1–B43 https://doi.org/10.3133/pp1035B

Pettigrew, R.P., Rogers, S.L. and Clarke, S.M., (2020). A microfacies analysis of arid continental carbonates from the Cedar Mesa Sandstone Formation, Utah, USA. The Depositional Record, 6(1), pp.41-61. https://doi.org/10.1002/dep2.99

Pettigrew, R.P., Priddy, C., Clarke, S.M., Warke, M.R., Stüeken, E.E. and Claire, M.W., (2021). Sedimentology and isotope geochemistry of transitional evaporitic environments within arid continental settings: From erg to saline lakes. Sedimentology, 68(3), pp.907-942. https://doi.org/10.1111/sed.12816

Phillips, S.P., Howell, J.A., Hartley, A.J. and Chmielewska, M., (2020). Tidal estuarine deposits of the transgressive Naturita Formation (Dakota Sandstone): San Rafael Swell, Utah, USA. Journal of Sedimentary Research, 90(8), pp.777-795. https://doi.org/10.2110/jsr.2020.51

Pipiringos, G.N., and O'Sullivan, R.B. (1978). Principal unconformities in Triassic and Jurassic rocks, western interior United States: a preliminary survey. U.S. Geological Survey, Professional Paper, 1035-A, 1-29. https://doi.org/10.3133/pp1035A

Porter, M.L., (1986). Sedimentary record of erg migration. Geology, 14(6), pp.497-500. https://doi.org/10.1130/0091-7613(1986)14%3C497:SROEM%3E2.0.CO;2

Priddy, C.L. and Clarke, S.M., (2020). The sedimentology of an ephemeral fluvial–aeolian succession. Sedimentology, 67(5), pp.2392-2425. https://doi.org/10.1111/sed.12706

Priddy, C.L. and Clarke, S.M., (2021). Spatial variation in the sedimentary architecture of a dryland fluvial system. Sedimentology, 68(6), pp. 2887-2917. https://doi.org/10.1111/sed.12876

Priddy, C.L., Pringle, J.K., Clarke, S.M. and Pettigrew, R.P., (2019). Application of photogrammetry to generate quantitative geobody data in ephemeral fluvial systems. The Photogrammetric Record, 34(168), pp.428-444. https://doi.org/10.1111/phor.12299

Priddy, C., Regis, A., Clarke, S., Leslie, A. and Dodd, T., (2021). Localized bank collapse or regional event? Geology of the Intermountain West, 8, pp.27-44. https://doi.org/10.31711/giw.v8.pp27-44

Purvis, K., (1991). Stoss-side mud-drapes: deposits of interdune pond margins. Sedimentology, 38(1), pp.153-156. https://doi.org/10.1111/j.1365-3091.1991.tb01860.x

Rankey, E.C., 1997. Relations between relative changes in sea level and climate shifts: Pennsylvanian–Permian mixed carbonate-siliciclastic strata, western United States. *Geological Society of America Bulletin,* 109(9), pp.1089-1100.

Rahman, M., Faupl, P., & Alam, M. M. (2009). Depositional facies of the subsurface Neogene Surma Group in the Sylhet Trough of the Bengal Basin, Bangladesh: record of tidal sedimentation. International Journal of Earth Sciences, 98(8), 1971-1980. https://doi.org/10.1007/s00531-008-0347-7

Reesink, A. J., andBridge, J. S. (2011). Evidence of bedform superimposition and flow unsteadiness in unit-bar deposits, South Saskatchewan River, Canada. Journal of Sedimentary Research, 81(11), 814-840. https://doi.org/10.2110/jsr.2011.69

Reineck, H.E. and Wunderlich, F., 1968. Classification and origin of flaser and lenticular bedding. *Sedimentology*, *11*(1-2), pp.99-104. https://doi.org/10.1111/j.1365-3091.1968.tb00843.x

Rodríguez-López, J.P., Peyrot, D. and Barrón, E., 2020. Complex sedimentology and palaeohabitats of Holocene coastal deserts, their topographic controls, and analogues for the mid-Cretaceous of northern Iberia. *Earth-Science Reviews*, 201, p.103075.

Rodríguez-López, J.P., Clemmensen, L.B., Lancaster, N., Mountney, N.P. and Veiga, G.D., (2014). Archean to Recent aeolian sand systems and their sedimentary record: current understanding and future prospects. Sedimentology, 61(6), pp.1487-1534. https://doi.org/10.1111/sed.12123

Rodríguez-López, J.P., Meléndez, N., de Boer, P.L., Soria, A.R. and Liesa, C.L., (2013). Spatial variability of multi-controlled aeolian supersurfaces in central-erg and marine-erg-margin systems. Aeolian Research, 11, pp.141-154. https://doi.org/10.1016/j.aeolia.2013.07.002

Rodríguez-López, J.P., Melendez, N., De Boer, P.L. and Soria, A.R., (2012). Controls on marine–erg margin cycle variability: aeolian–marine interaction in the mid-Cretaceous Iberian Desert System, Spain. Sedimentology, 59(2), pp.466-501 https://doi.org/10.1111/j.1365-3091.2011.01261.x

Rodríguez-López, J.P. (2008) Sedimentología y Evolución del Sistema Desértico Arenoso (erg) Desarrollado en el Márgen Occidental del Tethys Durante el Cretácico Medio. Cordillera Ibérica. Provincias de Teruel y Zaragoza. Unpublished PhD Thesis, Universidad Complutense de Madrid-Consejo Superior de Investigaciones Científicas, 500 pp.

Sass, I. and Götz, A.E., 2012. Geothermal reservoir characterization: a thermofacies concept. *Terra Nova*, *24*(2), pp.142-147 https://doi.org/10.1111/j.1365-3121.2011.01048.x

Sato, T., Taniguchi, K., Takagawa, T., & Masuda, F. (2011). Generation of tidal bedding in a circular flume experiment: Formation process and preservation potential of mud drapes. Geo-Marine Letters, 31(2), pp. 101-108. https://doi.org/10.1007/s00367-010-0218-7

Scorgie, J.C., Worden, R.H., Utley, J.E.P. and Roche, I.P., (2021). Reservoir quality and diagenesis of Triassic sandstones and siltstones from arid fluvial and playa margin environments: A study of one of the UK's earliest producing oilfields. Marine and Petroleum Geology, 131, p.105154. https://doi.org/10.1016/j.marpetgeo.2021.105154

Sharp, R.P., 1963. Wind ripples. *The Journal of Geology*, *71*(5), pp.617-636. https://doi.org/10.1086/626936

Storms, J. E. (2003). Event-based stratigraphic simulation of wave-dominated shallow-marine environments. Marine Geology, 199(1-2), 83-100. https://doi.org/10.1016/S0025-3227(03)00144-0

Svendsen, J., Friis, H., Stollhofen, H. and Hartley, N., 2007. Facies discrimination in a mixed fluvio-eolian setting using elemental whole-rock geochemistry—applications for reservoir characterization. Journal of Sedimentary Research, 77(1), pp.23-33. https://doi.org/10.2110/jsr.2007.008

Tabor, N.J., Myers, T.S. and Michel, L.A., (2017). Sedimentologist's guide for recognition, description, and classification of paleosols. In Terrestrial Depositional Systems (pp. 165-208). Elsevier. https://doi.org/10.1016/B978-0-12-803243-5.00004-2

Taggart, S., Hampson, G.J. and Jackson, M.D., (2010). High-resolution stratigraphic architecture and lithological heterogeneity within marginal aeolian reservoir analogues. Sedimentology, 57(5), pp.1246-1279. https://doi.org/10.1111/j.1365-3091.2010.01145.x

Tanner, W.F., 1964. Eolian ripple marks in sandstone. *Journal of Sedimentary Research*, *34*(2), pp.432-433. https://doi.org/10.1306/74D710A0-2B21-11D7-8648000102C1865D

Tessier, E. (2022). Tidal rhythmites: Their contribution to the characterization of tidal dynamics and environments. In: Green, M. & Duarte, J.C. (eds), A Journey Through Tides, 283-305. https://doi.org/10.1016/B978-0-323-90851-1.00015-7

Thompson AE, Stokes WL. (1970). Stratigraphy of the San Rafael group, southwest and south central Utah. Utah Geological and Mineralogical Survey, Bulletin. 87:1–50.

Thorman, C. H. (2011). The Elko orogeny–A major tectonic event in eastern Nevada–western Utah. Sevier thrust belt—northern and central Utah and adjacent areas. In Sprinkel, D.A., Yonkee, W.A., and Chidsey, T.C. Jr. (Eds.), Sevier Thrust Belt: Northern and Central Utah and Adjacent Areas, Utah Geological Association, Publication 40, 117-129.

Trewin, N.H., (1993). Controls on fluvial deposition in mixed fluvial and aeolian facies within the Tumblagooda Sandstone (Late Silurian) of Western Australia. Sedimentary Geology, 85(1-4), pp.387-400. https://doi.org/10.1016/0037-0738(93)90094-L

Valenza, J.M., 2016. Redbeds of the Upper Entrada Sandstone, Central Utah: facies analysis and regional implications of interfingered sabkha and fluvial terminal splay sediments. Brigham Young University.

Wakefield, O.J. and Mountney, N.P., 2013. Stratigraphic architecture of back-filled incised-valley systems: Pennsylvanian–Permian lower Cutler beds, Utah, USA. Sedimentary Geology, 298, pp.1-16.

Wilcox, W.T., and Currie, B. (2008). Sequence Stratigraphy of the Jurassic Curtis, Summerville, and Stump formations, Eastern Utah and Northwest Colorado. In: Longman, M.W., and Morgan, C.D. (Eds.), Hydrocarbon Systems and Production in the Uinta Basin, Utah, Rocky Mountain Association of Geologists and Utah Geological Association, Publication 37, 9-41.

Wilson, I.G., (1972). Aeolian bedforms—their development and origins. Sedimentology, 19(3-4), pp.173-210. https://doi.org/10.1111/j.1365-3091.1972.tb00020.x

Witkind, I.J., 1988. Geologic map of the Huntington 30'X 60'quadrangle, Carbon, Emery, Grand, and Uintah Counties, Utah (No. 1764).

Wright, J.C., Shawe, D.R. and Lohman, S.W., (1962). Definition of members of Jurassic Entrada Sandstone in east-central Utah and west-central Colorado. AAPG Bulletin, 46(11), pp.2057-2070. https://doi.org/10.1306/BC74394B-16BE-11D7-8645000102C1865D

Yang, B. C., Dalrymple, R. W., & Chun, S. S. (2005). Sedimentation on a wave-dominated, open-coast tidal flat, south-western Korea: summer tidal flat–winter shoreface. Sedimentology, 52(2), 235-252. https://doi.org/10.1111/j.1365-3091.2004.00692.x

Yu, X., Li, S. and Li, S., 2018. *Clastic Hydrocarbon Reservoir Sedimentology*. Springer. https://doi.org/10.1007/978-3-319-70335-0

Yu, X., Liu, C., Wang, C., & Wang, J. (2021). Late Cretaceous aeolian desert system within the Mesozoic fold belt of South China: Palaeoclimatic changes and tectonic forcing of East Asian erg development and preservation. Palaeogeography, Palaeoclimatology, Palaeoecology, 567, 110299. https://doi.org/10.1016/j.palaeo.2021.110299

Zuchuat, V., Sleveland, A., Sprinkel, D., Rimkus, A., Braathen, A., and Midtkandal, I. (2018). New insights on the impact of tidal currents on a low-gradient, semi-enclosed, epicontinental basin—the Curtis Formation, east-central Utah, USA. Geology of the Intermountain West, 5, 131-165. https://doi.org/10.31711/giw.v5.pp131-165

Zuchuat, V., Sleveland, A.R., Pettigrew, R.P., Dodd, T.J., Clarke, S.M., Rabbel, O., Braathen, A. and Midtkandal, I. (2019a). Overprinted allocyclic processes by tidal resonance in an epicontinental basin: The Upper Jurassic Curtis Formation, east-central Utah, USA. The Depositional Record, 5(2), 272-305. https://doi.org/10.1002/dep2.69

Zuchuat, V., Midtkandal, I., Poyatos-Moré, M., Da Costa, S., Brooks, H.L., Halvorsen, K., Cote, N., Sundal, A., and Braathen, A. (2019b). Composite and diachronous stratigraphic surfaces in low-gradient, transitional settings: The J-3 "unconformity" and the Curtis Formation, east-central Utah, USA. Journal of Sedimentary Research, 89(11), 1075-1095. https://doi.org/10.2110/jsr.2019.56

Zuchuat, V., Steel, E., Mulligan, R.P., Collins, D.S. and Green, J.M. (2022), Tidal dynamics in palaeo-seas in response to changes in physiography, tidal forcing and bed shear stress. Sedimentology. Accepted Author Manuscript. https://doi.org/10.1111/sed.12975

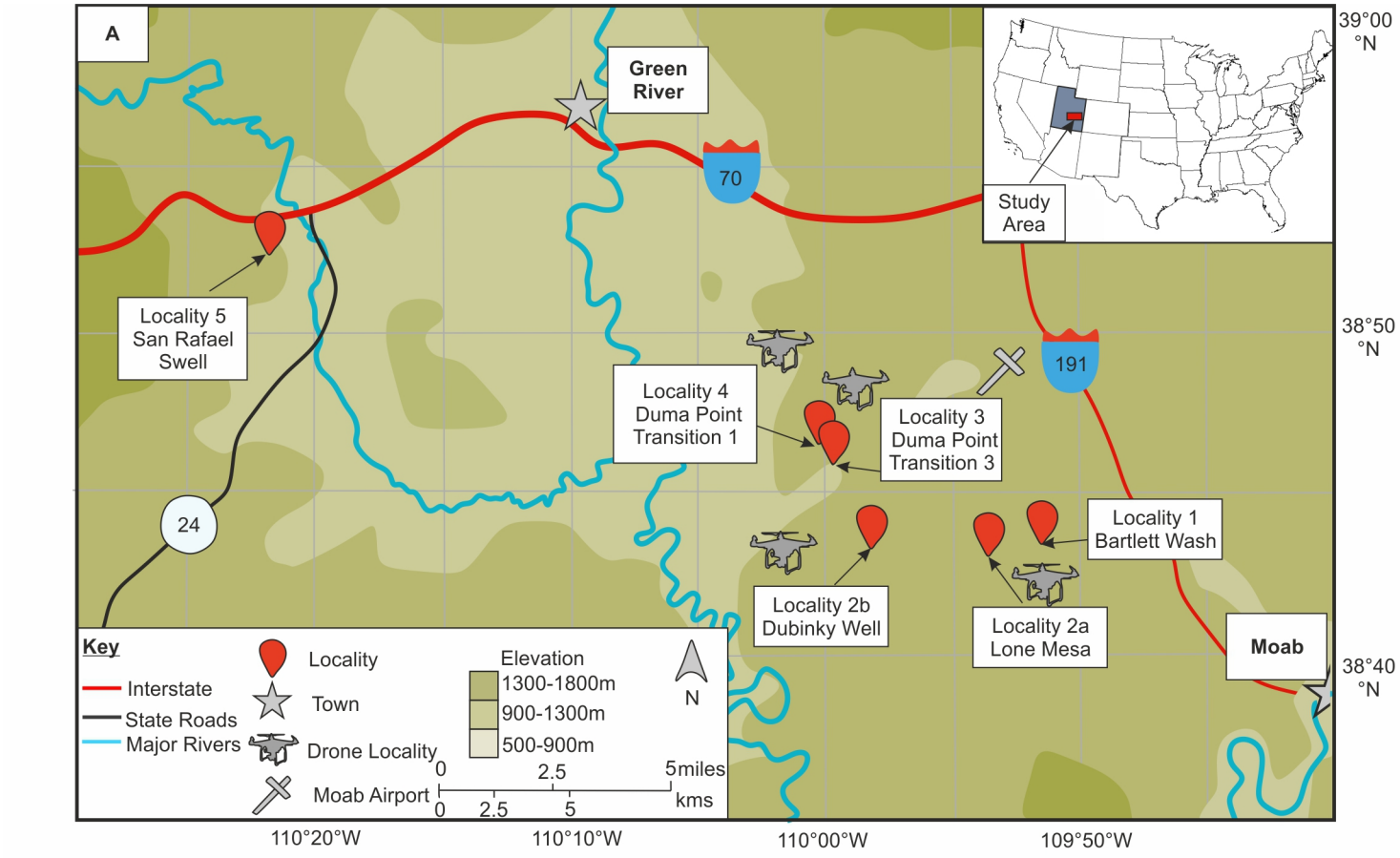

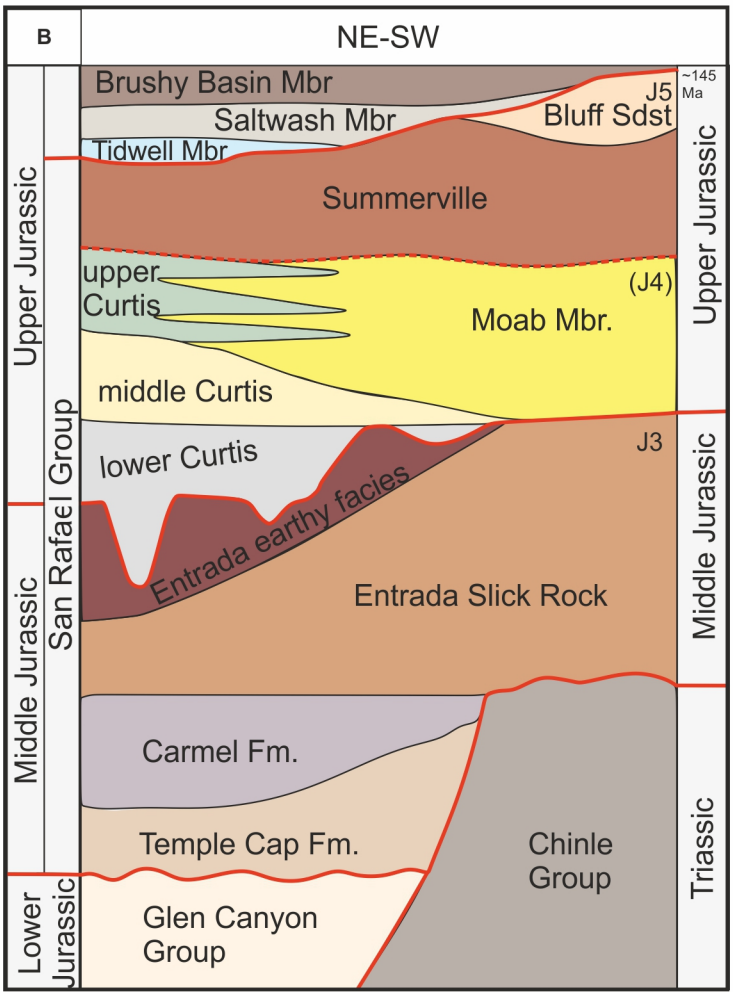

C Log no.	Log Name	UTM Coordinates		
		Grid	Easting	Northing
1	Bartlett Wash	12S	060007	4286108
2a	Lone Mesa	12S	0601637	4281798
2b	Dubinky Well	12S	0595320	4284581
3	Duma Point Transition 3	12S	0576847	4330039
4	Duma Point Transition 1	12S	0590497	4293490
5	San Rafael Swell	12S	0550383	4308262

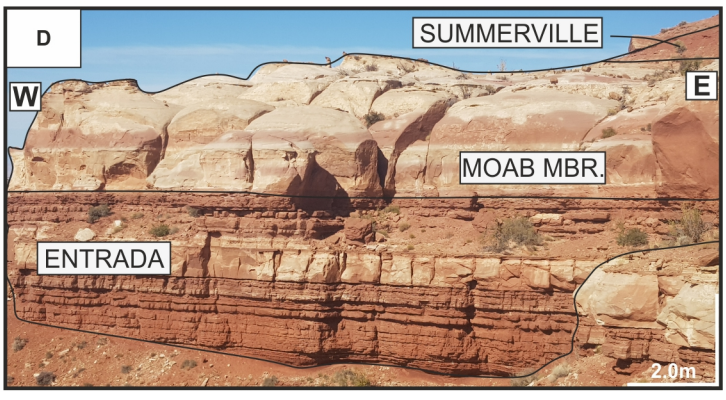

DEP2_225_Figure 1.jpg

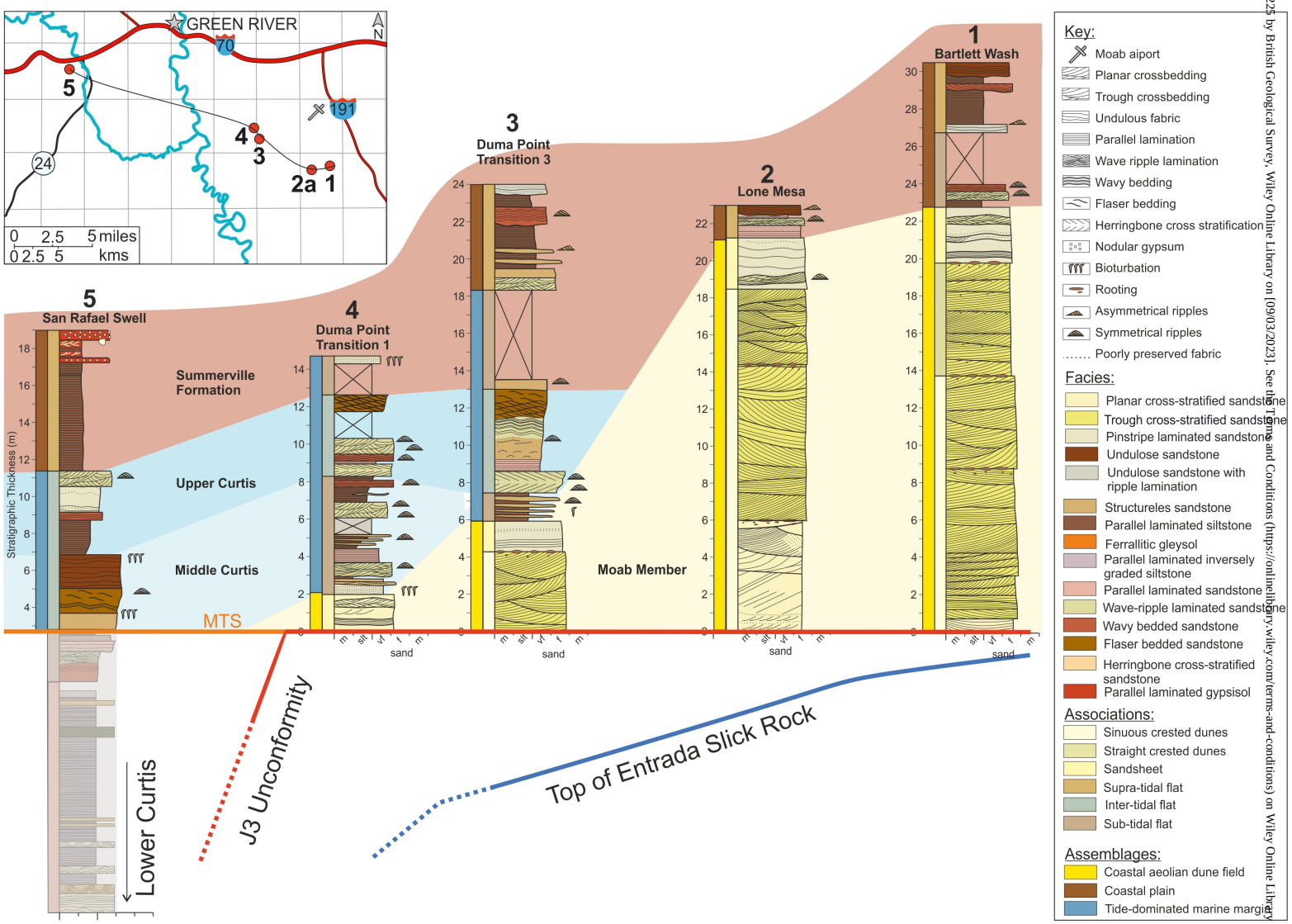

DEP2_225_Figure 2.jpg

DEP2_225_Figure 3.jpg

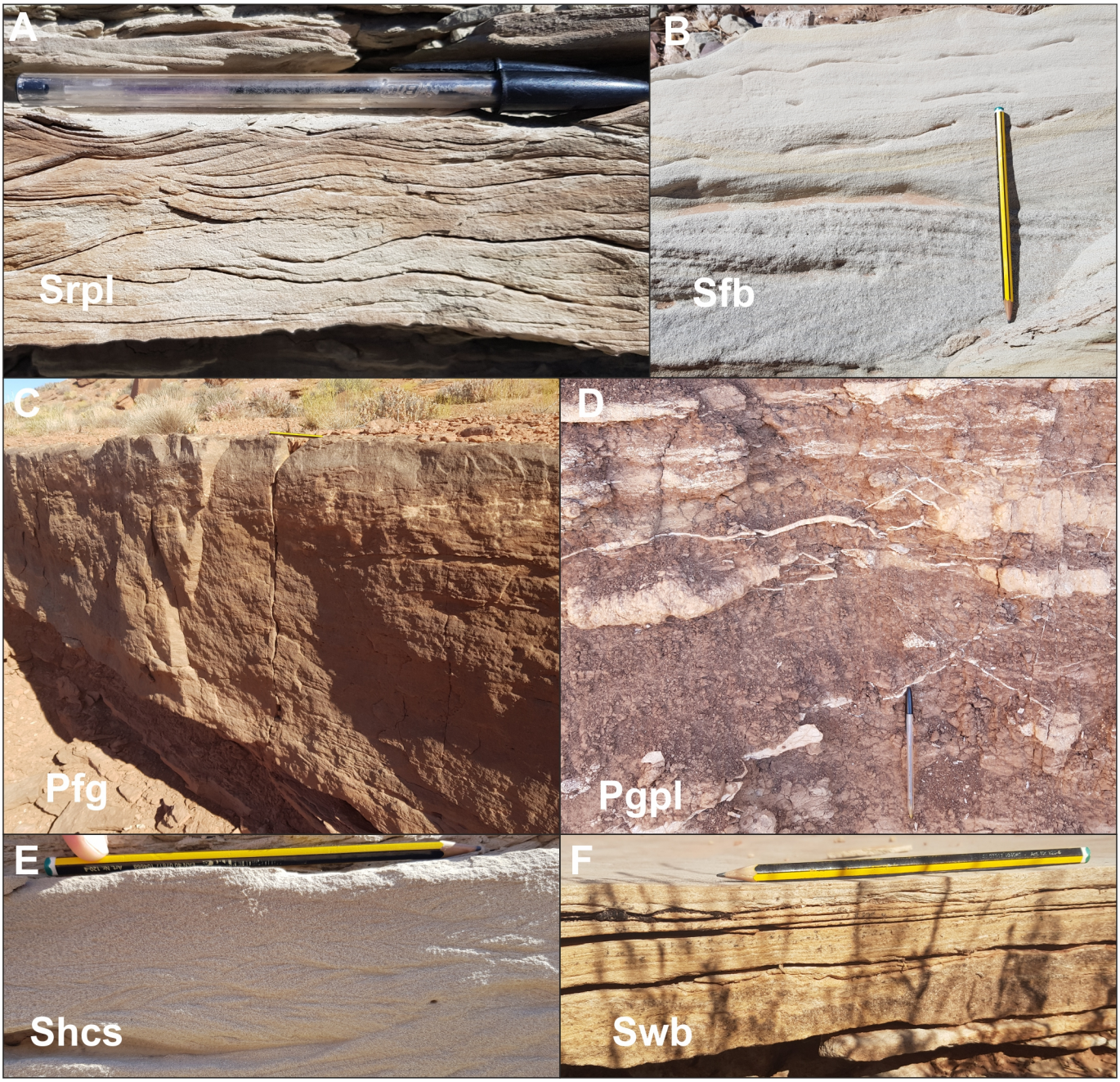

DEP2_225_Figure 4.jpg

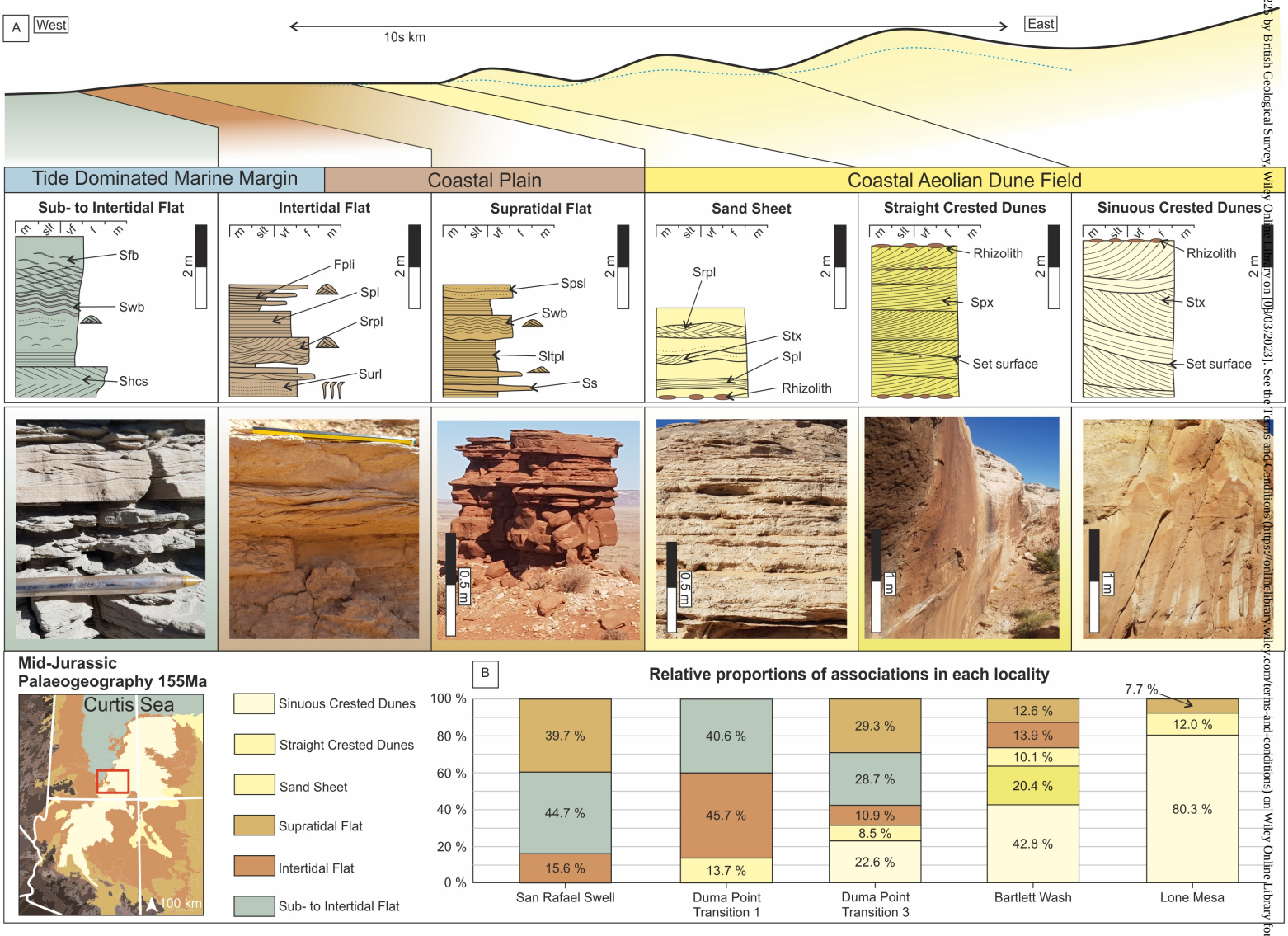

DEP2_225_Figure 5.jpg

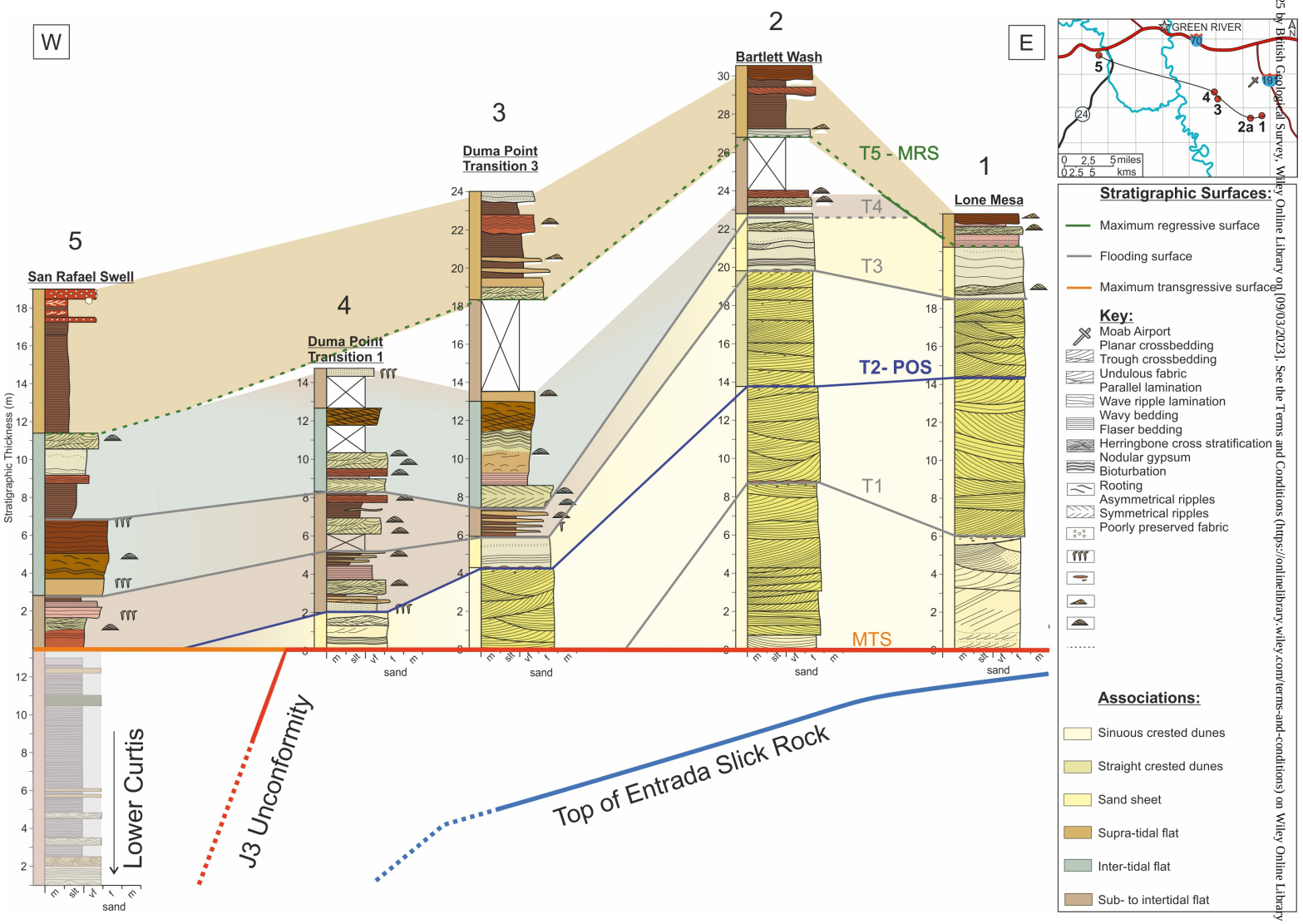

DEP2_225_Figure 6.jpg

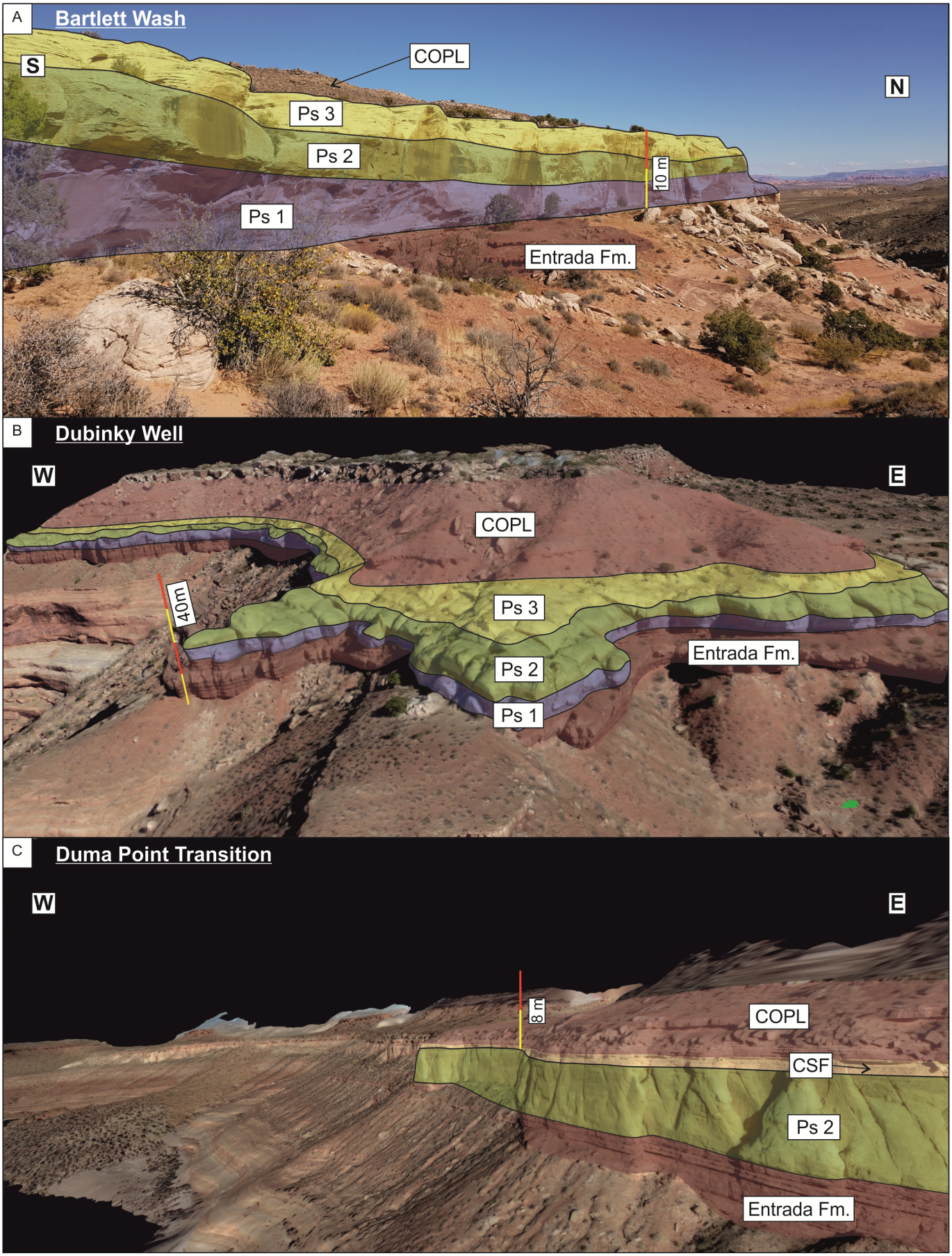

DEP2_225_Figure 7.jpg

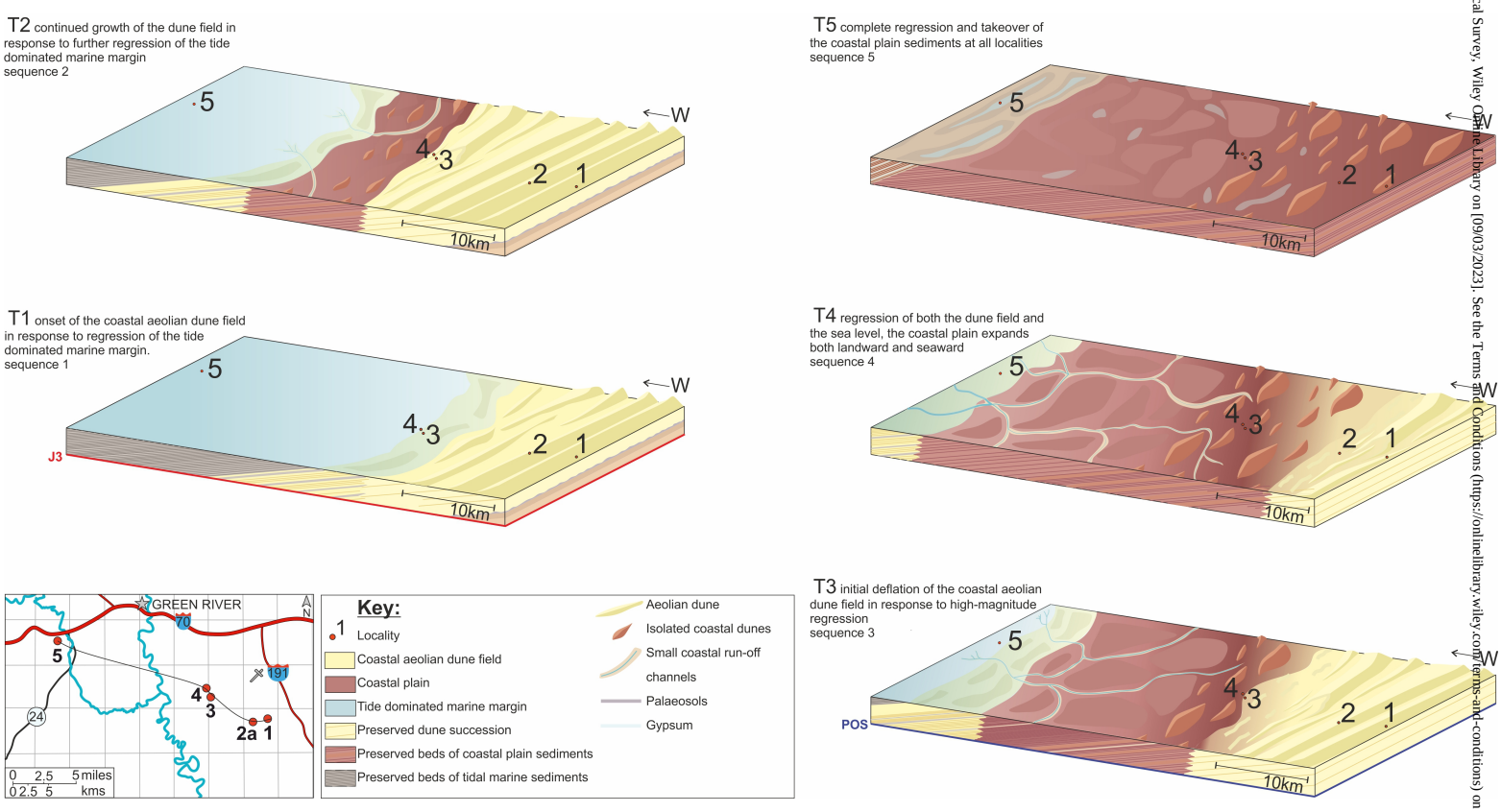

DEP2_225_Figure 8.jpg

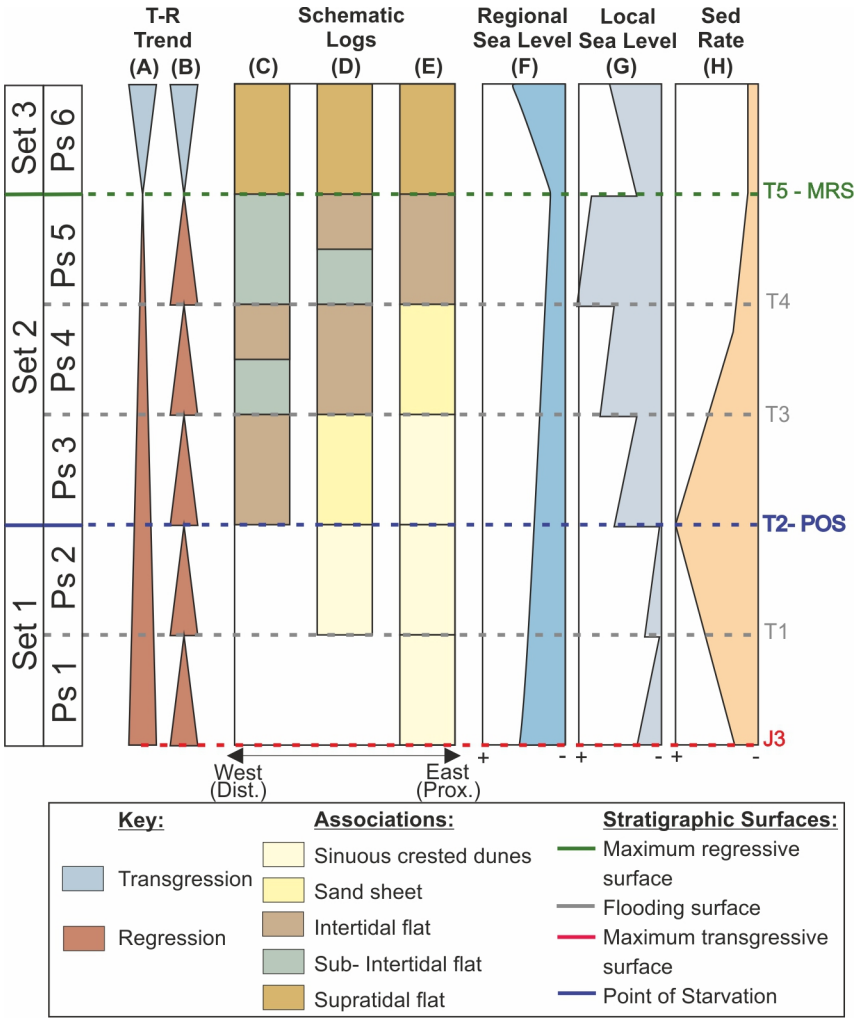

DEP2_225_Figure 9.jpg

Facies	Description	Interpretation
Planar cross-stratified sandstones (Spx)	Yellow, pale cream planar cross-bedded sandstones, medium-grained and well sorted, well-rounded. At the base of the foresets, there is evidence of inverse grading of slightly coarser grains separated by fine-grained laminae. Rhizolith horizons occur along set-bounding surfaces at the base of the facies. Foresets are truncated at the top, asymptotic at the base with thicknesses ranging from millimetre to centimetre-scale. Foreset bases truncate against parallel set bounding surfaces approximately 1 m apart, stacked into cosets with a maximum thickness of 1-19 m.	Straight-crested dune-scale bedforms migrating as dune trains. Inverse graded and fine-grained laminae represent grainflow and grainfall, respectively. Planar set bounding surfaces indicate straight-crested dune forms (McKee & Wier 1953, Hunter 1977, Trewin, 1993; Ewing & Kocurek, 2010, Collinson & Mountney, 2019). Rhizolith horizons demonstrate periods of stabilisation within which vegetation can prevail upon dune slopes (Mountney & Thompson, 2002).
Trough cross-stratified sandstones (Stx)	Light grey to light pink trough cross-bedded sandstones, fine- to medium-grained, well sorted and well-rounded, with an average grain size of fine sand. At the base of the foresets, there is evidence of inverse grading of slightly coarser grains separated by fine-grained laminae. Foresets are truncated at the top, asymptotic at the base with thicknesses ranging from millimetre to centimetre-scale. The set-bounding surfaces truncate the tops of the foresets and meet at the base asymptotically; at outcrop scale, they have a convex or curved profile. Set thicknesses can reach up to 2 m and build into cosets no larger than 5 m.	Sinuous-crested dune-scale bedforms created by wind-blown sands, migrating as dune trains. Inverse graded and fine-grained laminae represent grainflow and grainfall, respectively. The trough cross-bedded nature of strata but also the curved set bounding surfaces indicate sinuosity in bedform crests (McKee & Weir 1953, Hunter 1977, Crabaugh & Kocurek, 1993, Mountney, 2012, Banham et al., 2018).
Pinstripe-laminated sandstone (Spsl)	Light grey to reddish brown, fine-grained, well-sorted and well-rounded sandstone. Nearly horizontal laminations with bimodal sorting (pinstripe) represent subcritical translatent strata with sporadic shallowly climbing (<8°) ripple bedform laminae.	Wind ripples developed through rhythmic wind cycles in the lee of dunes (Sharp 1963, Tanner 1964, Fryberger & Schenk, 1988), rhythmic sediment incursions may also be associated with the preservation of internal ripple laminae and an increased angle of climb. It is interpreted that this is recycling of grainflow deposits (Banham et al., 2018) in dune lee slope toes.
Undulous Sandstone (Su)	Red-brown, moderately sorted, very fine- to fine-grained sandstone, with sporadic lenses of argillaceous material. Undulose bed bounding surfaces define inter-and intra-facies contacts, these beds (10-30 cm thick) undulate slightly vertically with metre scale wavelengths. Mostly structureless, internally, towards the top of the facies, mottling and water escape structures are prominent.	Wind-blown sediment deposited within very shallow standing water via suspension settlement (Mountney & Thompson, 2002). Argillaceous material, water escape structures and mottling are all products of depositional and diagenetic textures that indicate a high-water table during deposition. The undulose nature of bedding contacts can be interpreted as antecedent topography from the underlying facies (Desjardins et al., 2012) or induced by surface wave action (Martel & Gibling, 1991; Mountney & Thompson, 2002, Collinson & Mountney, 2019).
Undulous sandstone	Dark reddy-brown sandstone of fine- to medium-grainsize. The grains are sub-rounded and poorly sorted with a minority of clay particles. Internally, mud lenses	Wind-blown sediment deposited within very shallow standing water via suspension settlement (Mountney & Thompson, 2002).

with ripple laminations (Surl)	and mud drapes occur sporadically throughout the facies. Undulose bed bounding surfaces define inter-and intra-facies contacts, these beds (10-30 cm thick) undulate slightly vertically with metre scale wavelengths, with some small poorly preserved foresets at the base. Wave-ripple laminae are evident, sporadically, towards the top of the facies.	Mud drape material suggests settling of fines within the water column onto wind-blown sands during episodic and minor flood events (Purvis, 1991). Wave-ripple lamination indicates that wind speeds across the water-air interface are sufficient to generate oscillatory wind-ripples on the sediment-water surface (Mountney & Thompson, 2002). The undulose nature of bedding contacts can be interpreted as antecedent topography from the underlying facies (Desjardins et al., 2012) or induced by surface wave action (Martel & Gibling, 1991; Mountney & Thompson, 2002, Collinson & Mountney, 2019).
Structureless sandstone (Ss)	Red-cream argillaceous sandstone that forms 30-50 m wide and 0.5 to 1 m thick lenticular beds that are mostly structureless. When the facies top is preserved, poorly defined discontinuous asymmetrical ripple lamination can be observed. This facies is well cemented and bleached in some areas. The lower, concave-up bounding surface is commonly erosive and contains load casts and very sporadic rip-up clasts. No observable grading.	Episodic poorly channelised high sediment load non-Newtonian flows (Priddy & Clarke, 2020; Priddy *et al.,* 2021). Load casts at the base demonstrate rapid deposition onto a weaker substrate. Discontinuous ripples towards the top of the facies indicate waning of flow energy and sediment load, enabling lower flow regime deposition of minor bedforms.
Parallel-laminated siltstone (Sltpl)	Poorly consolidated, red-brown, poorly sorted, moderately rounded mud to siltstone interbedded with parallel laminated mudstone. At top of the facies, there is minor mottling and occasional poorly preserved vertical burrows. Minor evidence of cross cutting gypsum veins and nodules.	Suspension settling upon a flat surface. The mottling and burrowing are indicators of minor vegetation and habitation of deposited areas (Graziński & Uchman, 1994; Desjardins et al., 2012).
Parallel-laminated Gypsisol (Pgpl)	Brown to red in colour, poorly sorted, moderately rounded siltstone, Bkt horizon showing dark banding with minor mottling, some very thin gypsum lined horizontal lamination. Centimetre scale nodules of gypsum seen at the top of the horizon. By horizon, abrupt-smooth top bounding surface with By-Bkt horizon, pervasive satin-spar gypsum precipitation along parent laminations. Basal horizon, Bky is a nodular gypsum horizon with gypsum-filled slickensides, top bounding surface is abrupt-wavy.	Suspension settlement within calm shallow water creating parent sedimentary facies. Well drained gleyed vertic Gypsisol, deposited in an arid climate (Mack et al., 1993, Desjardins et al., 2012). Precipitation of evaporitic material from saline waters with mild illuviation of clay minerals in Bkt top horizon and lower Bky horizon (Tabor et al., 2017). This suggests periodic draw down of the water table, given the extensive presence of gypsum, the dominant process of draw-down is evapotranspiration. Vertic textures are produced by the high rate of evapotranspiration, leading to rapid shrink-swell contrasts (Milroy et al., 2018).

Ferrallitic Gleysol (Pfg)	Pale cream, poorly sorted, poorly consolidated sandstone with red/brown mottles throughout. Structureless, with no evidence of bioturbation and rooting. Grey concretions along the base of the facies. Due to its mottled appearance and nodular surface texture composed of amorphous sesquioxides, this facies is colloquially termed the 'popcorn facies' within the literature (Zuchuat *et al*., 2019).	Gleysol developed through fluctuating water table, not controlled by evapotranspiration, but the migration of interstitial waters leading to gleying and illuviation (Mack *et al.,* 1993, Desjardins et al., 2012, Tabor *et al.,* 2017). Quiescent periods of drainage lead to the development of amorphous nodular growth and mottled oxidisation (Buol & Eswaran, 1999).
Parallel-laminated inversely-graded siltstone (Slti)	Siltstone, inverse graded into very fine-grained sandstone towards the top of the unit. Parallel laminated with small fluctuations in grainsize between laminae. Grains are well-sorted and well-rounded and form beds of uniform thickness. Contacts between beds are slightly undulose and are typically poorly consolidated.	The grain size and contacts between the beds are strong indicators of suspension settlement within shallow-moderate depth water (Flemming, 2011). The difference in grain size suggests rapidly fluctuating energy levels or calibre of sediment falling out of suspension (Collinson & Mountney, 2018). However, the general reverse-grading trend also implies an increase in energy upwards, associated with a decrease in water depth or increase in flow speed.
Parallel-laminated sandstone (Spl)	Pink, very fine-grained sandstone that is well-sorted and moderately well-rounded. The grainsize coarsens upwards from very fine-grained at the base to fine-medium sand at the top. Beds typically thicken upwards, mostly parallel laminated internally. Facies are typically 1m thick showing parallel bedding with slightly undulose contacts between the beds.	Tractional laminations formed by turbulent flow at the limit between lower and upper flow regime . The reverse grading and thickening of the beds upwards implies a decrease in flow depth or increase in flow speed therefore increasing the transport capacity of the flow.
Wave-ripple-laminated sandstone (Srpl)	Light grey, moderately sorted, moderately rounded, very fine- to fine-grained sandstone. Uniform lamination turning into irregular interfingering ripple lamination, with evidence of bundled up-building and chevron style up-building. Variable directional asymmetrical ripple strata commonly juxtaposing one another, with undulating lower boundary sets and offshoot draping foresets. Some flame structures can be seen sporadically, although often relatively small (mm) in scale. There are also clear foresets that can be seen intersecting within the ripples themselves.	Wind action acting upon a water surface forms eddies which act upon suspension settled sand beds causing the ripple formation to gradually propagate upwards (Raff et al., 1977; Collinson & Mountney, 2019), creating wave ripples.

Wavy-bedded sandstone (Swb)	Light grey, moderately sorted, moderately- to well-rounded very fine- to fine-grained sandstone. Irregular undulous lamination with poorly preserved asymmetrical ripple forms. Siltstone laminations are present over ripple top bounding surfaces and basal set surfaces, preserving as siltstone in an undulous and wavy fabric.	Alternations of mud and sand reflect regular but long term (weeks to months) energy level variations in a lower flow regime setting (Allen, 1984), under which sinuous-crested ripples were migrating through tractional reworking of sediment (lower flow regime) (Baas et al., 2016).
Flaser-bedded sandstone (Sfb)	Grey, moderately to well sorted, moderately- to well-rounded fine-grained sandstone. Irregular undulous laminations of siltstone can be found throughout. Unidirectional trough cross-stratified forms can be seen throughout, draped on their foresets with siltstone (both single and double drapes). Base of the facies is characterised by double drapes, whereas simple drapes become more common upwards.	Unidirectional migration of sinuous-crested ripples through tractional reworking of sediment (lower flow regime), with mud drapes on the foresets of the sand ripples testify of abrupt drop in energy level, potentially reflecting tidal processes (Baas et al., 2016)
Unidirectional rippled to herringbone cross-stratified sandstone (Shcs)	Yellow-grey, moderately sorted, sub-rounded, argillaceous, very fine- to fine-grained sandstone. The internal structure at the top and base of the facies consists of occasional trough cross-stratification; however, internally a large percentage of the bedding can be identified as bidirectional trough cross-stratification.	Unidirectional to bidirectional migration of sinuous-crested ripples through tractional reworking of sediment (lower flow regime), with bidirectionality potentially reflecting tidal processes (Baas et al., 2016)

Facies Association	Constituent Facies	Description	Interpretation	Facies Belt
Sinuous crested dunes (FA1)	Stx, Spsl	Tabular bodies composed of trough cross-bedded sandstones (Stxs) stacked into sets (1-5 m), that interfinger with thin deposits of pinstripe-laminated sandstones (Spsl). Set surfaces are convex-up with relatively planar coset surfaces that extend beyond the outcrop.	Aeolian sinuous crested dunes, given the pervasive deposition of grainfall and grainflow strata combined with the convex-up geometry of set bounding surfaces (Banham et al., 2018). Wind ripples along dune toesets suggest winds with sufficient energy for traction to dominate in the lee of dune bedforms (Kocurek, 1991).	Coastal Aeolian Dune Field
Straight crested dunes (FA2)	Spx, Spsl	Tabular bodies composed of planar cross-bedded sandstones (Spx) stacked into sets with low-angle planar bounding surfaces. Cosets are up to 5 m thick, with coset bounding surfaces that are extremely planar and low angle extending laterally beyond the outcrop. Rhizoliths are sporadically identified along foresets, towards the top of sets.	Aeolian straight crested dunes, given the pervasive deposition of grainfall and grainflow strata combined with the planar geometry of set bounding surfaces (Mountney & Thompson, 2002). Wind ripples along dune toesets suggest winds with sufficient energy for traction to dominate in the lee of dune bedforms (Kocurek, 1991). Rhizolith development on foresets and towards set tops indicates primitive vegetation on the dune lee and dune crests.	Coastal Aeolian Dune Field
Sand sheet (FA3)	Su, Spsl, Stx, Pfg	Thick sheet-like bodies with planar to undulose bounding surfaces, dominated by undulose sandstones (Su) and sporadic occurrences of trough cross-bedded sandstone (Stx) and pinstripe laminated sandstone (Spsl). Towards the top of the succession, a ferric gleysol is seen (Pfg).	Sand sheet facies formed by being starved of sediment due to fluctuations in the water table (Mountney & Jagger, 2004). Fluid escape structures in the undulous bedded sandstones and illuviation of a ferric gleysol, suggest a high water table, but minor trough cross-bedded sandstones of aeolian origin suggest periods of low water table and sediment starvation.	Coastal Aeolian Dune Field to Coastal Plain
Supra-tidal flat (FA4)	Spl, Ss, Stx, Pgpl, Sltpl	Tabular bodies of parallel-laminated siltstones and sandstones (Sltpl & Spl) and erosionally based structureless sandstones (Ss) comprise the majority of the association, with isolated occurrences of trough cross-stratified sandstones (Stx) and a single occurrence of planar-laminated gypsisol (Pgpl) at the top of the association.	Arid supra-tidal flat occasionally flooded by the sea. Parallel-laminated siltstones and sandstones were deposited by suspension settling of wind-blown particles, with trough cross-stratified sandstones representing the migration of isolated, sinuous-crested dunes. Occasional structureless sandstones with a concave-up and erosive base represent channelised flash deposition of high sediment loads (Zuchuat et al., 2019). Evaporites indicate a high water table and sufficient exposure to have drawn down by evapotranspiration.	Coastal Plain to Tide-Dominated Shallow Marine
Intertidal flat (FA5)	Sltpl, Spl, Surl, Swb, Srpl	Planar laminated siltstones (Sltpl) interbedded with rippled undulose sandstones (Surl), overlain by wave-ripple laminated sandstone facies (Srpl) and wavy bedded sandstones (Swb). Planar laminated sandstones (Spl) can be seen towards the top of the succession.	Sand-rich intertidal flat sedimentation produced by tidal fluctuations in water level (Kvale, 2012). A rising water table deposits inversely-graded (with regards to laminae thickness) undulose and rippled sandstones (Zuchuat et al., 2018). Bedding planes commonly display sinuous out-of-phase ripples.	Tide-Dominated Shallow Marine

Sub- to intertidal flat (FA6)	Shcs, Swb, Sfb, Slti, Spl, Srpl	Tabular bodies of parallel-laminated, inversely-graded siltstones (Slti), grading into parallel laminated sandstones (Spl). Towards the top of the association wavy-bedded (Swb), flaser-bedded (Sfb), symmetrical ripple-cross-laminated sandstones (Srpl), and unidirectional ripple- to herringbone cross-stratified sandstones (Shcs) are abundant.	Sub- to intertidal flat dominated by suspension settlement and bidirectional flow deposits, evidencing changes in flow depth and depositional energy through alternating settlement grain sizes. Herringbone cross-stratification indicates the migration of dune deposits in two directions evidencing minor tidal influence (Zuchuat et al., 2019; Philips et al., 2020). The presence of mud draping on flaser and wavy bedding provides further evidence of tidal influence to the deposits.	Tide-Dominated Shallow Marine